HHS Public Access

Author manuscript

Cell Rep. Author manuscript; available in PMC 2023 March 06.

Published in final edited form as:

Cell Rep. 2023 January 31; 42(1): 111999. doi:10.1016/j.celrep.2023.111999.

Palmitoylation and PDE6δ regulate membrane-compartment-specific substrate ubiquitylation and degradation

David Liang[1,6], **Liping Jiang**[1,6], **Sameer Ahmed Bhat**[1], **Sonia Missiroli**[2], **Mariasole Perrone**[2], **Angela Lauriola**[3], **Ritika Adhikari**[1], **Anish Gudur**[1], **Zahra Vasi**[1], **Ian Ahearn**[4], **Daniele Guardavaccaro**[3], **Carlotta Giorgi**[2], **Mark Philips**[5], **Shafi Kuchay**[1,7,*]

[1]Department of Biochemistry and Molecular Genetics, University of Illinois at Chicago, MBRB #1157, Chicago, IL 60607, USA

[2]Department of Medical Sciences, Section of Experimental Medicine, University of Ferrara, 44121 Ferrara, Italy

[3]Department of Biotechnology, University of Verona, 37134 Verona, Italy

[4]Department of Dermatology and Perlmutter Cancer Center, New York University Grossman School of Medicine, New York, NY 10016, USA

[5]Department of Medicine and Perlmutter Cancer Center, New York University Grossman School of Medicine, New York, NY 10016, USA

[6]These authors contributed equally

[7]Lead contact

SUMMARY

Substrate degradation by the ubiquitin proteasome system (UPS) in specific membrane compartments remains elusive. Here, we show that the interplay of two lipid modifications and PDE6δ regulates compartmental substrate targeting via the SCF^{FBXL2}. FBXL2 is palmitoylated in a prenylation-dependent manner on cysteines 417 and 419 juxtaposed to the CaaX motif. Palmitoylation/depalmitoylation regulates its subcellular trafficking for substrate engagement and degradation. To control its subcellular distribution, lipid-modified FBXL2 interacts with PDE6δ.

*Correspondence: kuchay@uic.edu.

AUTHOR CONTRIBUTIONS

D.L., conceptualization, performed most of the biochemical, cell genetics, and imaging experiments, statistical analysis, participated in writing the original draft, literature survey, and prepared figures. L.J., performed biochemical fractionations, performed biochemical experiments, imaging, and statistical analysis along with D.L., helped with the validation of Flp-In cell system for inducible expression of FBXL2 and its mutants developed by S.A.B. and A.G., and prepared figures along with D.L. S.A.B., performed prenylation assays, developed Flp-In cell system with A.G., performed biochemical fractionations, and helped in figure preparations. S.M., M. Perrone, and C.G., performed calcium mobilization assays and their statistical analyses. A.L. and D.G., performed initial screenings for F box proteins. R.A., participated in development of radioactive prenylation assay along with S.A.B. and D.L. A.G., developed Flp-In cell system for FBXL2 and its mutants. Z.V., participated in confocal imaging of FBXL2 upon drug treatment with S.A.B. I.A. and M. Philips, manuscript editing, reviewing, and discussions. S.K., supervision, conceptualization, manuscript writing, and review and editing with D.L.

DECLARATION OF INTERESTS

The authors declare no competing interests.

SUPPLEMENTAL INFORMATION

Supplemental information can be found online at https://doi.org/10.1016/j.celrep.2023.111999.

Perturbing the equilibrium between FBXL2 and PDE6δ disrupts the delivery of FBXL2 to all membrane compartments, whereas depalmitoylated FBXL2 is enriched on the endoplasmic reticulum (ER). Depalmitoylated FBXL2(C417S/C419S) promotes the degradation of IP3R3 at the ER, inhibits IP3R3-dependent mitochondrial calcium overload, and counteracts calcium-dependent cell death upon oxidative stress. In contrast, disrupting the PDE6δ-FBXL2 equilibrium has the opposite effect. These findings describe a mechanism underlying spatially-restricted substrate degradation and suggest that inhibition of FBXL2 palmitoylation and/or binding to PDE6δ may offer therapeutic benefits.

In brief

Liang et al. show that FBXL2-CRL is palmitoylated at C417 and C419 juxtaposed to CaaX-prenylation-motif. Lipid-modified-FBXL2 in complex with PDE6δ regulates subcellular distribution. Perturbing FBXL2-PDE6δ equilibrium disrupts delivery of FBXL2 to all membrane compartments, whereas depalmitoylated FBXL2(C417S/C419S) is enriched at the ER. Spatially-restricted substrate engagement/degradation mechanism via FBXL2 is described.

Graphical Abstract

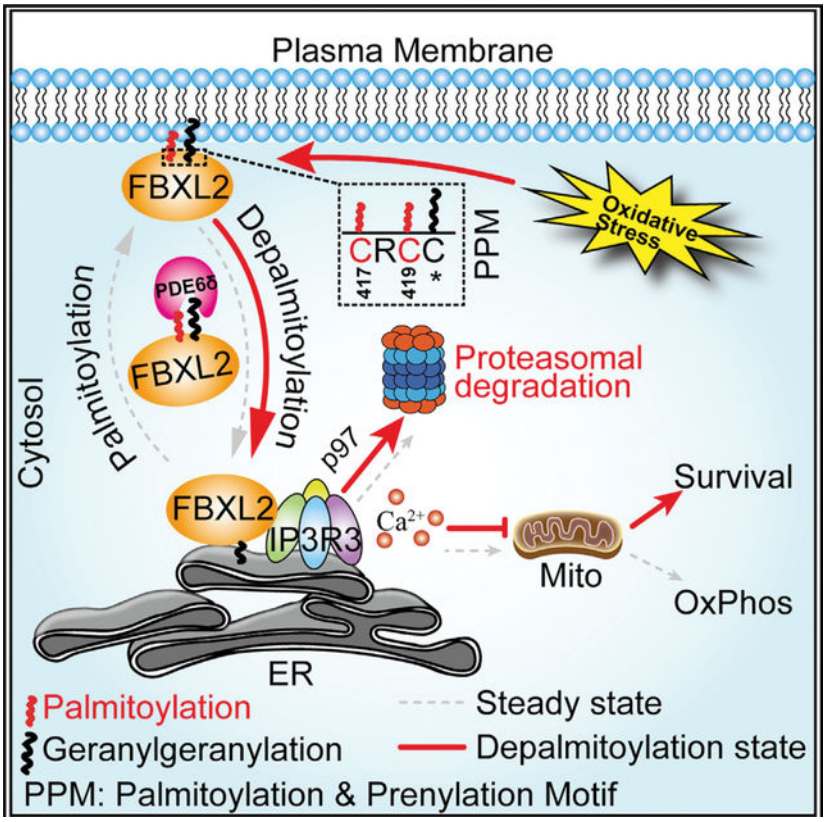

INTRODUCTION

Thousands of protein substrates undergo degradation via the ubiquitin proteasome system (UPS). The UPS operates in several different cellular compartments, including the cytosol

and nucleoplasm as well as membrane compartments such as endoplasmic reticulum (ER) mitochondrial membranes, and the plasma membrane (PM).[1–4] Despite its well-established role in cytosolic and nuclear compartments, UPS-mediated protein turnover at membrane compartments is not completely understood. In particular, the mechanisms by which non-transmembrane E3s are targeted to membranes to facilitate ubiquitination of organellar proteins are not established. The typical UPS proteolysis cascade consists of three sequential enzymatic processes carried out by E1, E2, and E3 ubiquitin ligases that mark protein substrates with ubiquitin polymers that signal for degradation in the proteasome.[4] E3 ligases, numbering ~600 family members encoded in the human genome, directly bind and recruit UPS substrates.[5,6] How E3 ubiquitin ligases are delivered to specific subcellular compartment(s), maintain their spatial organization, and target membrane protein substrates is under investigation.

Protein lipidation is one way that peripheral membrane proteins are targeted to cellular membranes in a regulated fashion.[7–9] Among the various types of lipidation, prenylation and palmitoylation are well known for controlling spatial organization and the trafficking of proteins, including the RAS superfamily of small G proteins.[10–12] During prenylation, one of two isoprenoid lipids, 15-carbon farnesyl or 20-carbon geranylgeranyl, are irreversibly attached by a thioether linkage to a cysteine residue near the C terminus.[9] The best understood examples of prenylated proteins are a large class of proteins that end with a CaaX motif (cysteine, aliphatic, any amino acid). Isoprenylation of CaaX motifs targets proteins to endomembranes. To allow delivery to the PM, prenylated proteins require a second targeting motif, which is referred to as a second signal.[13] The most common second signal is palmitoylation. Palmitate (16 carbon acyl chain) is added to proteins by one of 23 palmitoylacyltransferases (PATs) encoded in mammalian genomes.[11] Because palmitate is incorporated through a thioester bond that is readily hydrolyzed by thioesterases, cycles of palmitoylation/depalmitoylation regulate the subcellular localization of integral and peripheral proteins.[14,15]

Besides reversible palmitoylation, the subcellular localization of prenylated proteins is also regulated by cytosolic prenyl-binding proteins that can shield the lipid in the aqueous environment of the cytosol and allow for delivery from one membrane compartment to another. Among such prenyl-binding proteins is the δ subunit of type 6 phosphodiesterase (PDE6δ) that is ubiquitously expressed and has numerous CaaX protein clients.[16–20] The structure of PDE6δ is similar to that of RhoGDI in that both proteins possess hydrophobic pockets between β sheets.[19,21,22]

The majority of CaaX proteins are small GTPases in the RAS superfamily. However, FBXL2 and FBXL20 are also CaaX proteins among ~600 E3 ubiquitin ligases, the latter a paralog of FBXL2 expressed in neurons.[23–25] FBXL2 is a conserved F box protein that recruits protein substrates for the E3 ubiquitin ligase Skp1, Cul1, F box cullin-ring ligase (SCF-CRL), promoting their polyubiquitylation and subsequent degradation.[23,26–31] We and others have established that FBXL2 is post-translationally modified by geranylgeranylation at C420 in its CVIL CaaX sequence.[23,32,33] We have previously shown that the geranylgeranylation of FBXL2 is necessary for its localization on cell membranes, assembly into an active SCF ubiquitin ligase complex, and interaction

with two membrane localized substrates: p85β (a regulatory subunit of the PI3-kinase [PI3K]) and an ER resident calcium channel, the inositol 1,4,5-trisphosphate receptor type 3 (IP3R3).[23,27,28] By preventing excessive calcium flux from the ER to the mitochondria and promoting efficient activation of PI3K signaling due to degradation of IP3R3 and p85β at their respective subcellular membrane compartments, FBXL2 plays a critical role in cell survival. Subsequent studies reported other membrane-localized substrates of FBXL2 and FBXL20.[24–26,29–31,34,35] However, the molecular mechanism(s) that regulates the subcellular localization of FBXL2 and how its dynamic redistribution affects turnover of substrates in specific compartments has not been determined. Here, we demonstrate that the subcellular localization, redistribution, and function of prenylated FBXL2 is regulated by the interplay between FBXL2 palmitoylation and prenylation and its interactions with PDE6δ.

RESULTS

FBXL2 is palmitoylated on cysteines 417 and 419

FBXL2 terminates with a CaaX motif that we have shown is geranylgeranylated.[27,32] Because prenylation is necessary but not sufficient for delivery of CaaX proteins to the PM, which often requires palmitoylation of upstream cysteines, we determined if FBXL2 is palmitoylated. Immunoprecipitation, SDS-PAGE, and autoradiography of GFP-FBXL2 from cells metabolically labeled with [^{3}H] palmitate revealed incorporation of label into wild-type FBXL2 but not prenylation-deficient FBXL2(C420S) (Figure 1A, top left panel). As a control, we observed incorporation of the label into GFP-HRAS but not GFP-HRAS(C181S/C184S), which lacks palmitate acceptor sites. A similar result was obtained for FLAG-FBXL2 but not FLAG-FBXL3, a paralog that lacks a CaaX sequence (Figure 1A, top right panel). Thus, FBXL2 is palmitoylated in a prenylation-dependent fashion. Inspection of the FBXL2 sequence reveals two cysteines (C417 and C419) immediately upstream of the CaaX sequence that are highly conserved across species and are therefore candidates for palmitoylation (Figure 1B). Mutating both of these cysteines to serine, GFP-FBXL2(C417S/C419S), eliminated the incorporation of [^{3}H] upon metabolic labeling with [^{3}H] palmitate, demonstrating that one or both of these cysteines is a palmitate acceptor (Figure 1C). To confirm FBXL2 palmitoylation and determine the relative contribution of C417 and C419, we employed acyl-biotin exchange (ABE) analysis using biotinBMCC, which allows affinity capture of palmitoylated proteins with streptavidin (Figure S1A). Upon ABE analysis, whereas GFP-FBXL2 was labeled with biotin, GFP-FBXL2(C417S/C419S) was not, confirming palmitoylation of one or both of these cysteines (Figures 1D and S1A). Eliminating either cysteine alone diminished, but did not abolish, palmitoylation of FBXL2, demonstrating that both C417 and C419 are palmitate acceptors, albeit to a varying extent (Figure 1D). Thus, FBXL2 can be modified with palmitate either on C417 or C419.

Palmitoylation is prenylation dependent and regulates FBXL2 subcellular distribution

Having demonstrated that palmitoylation of FBXL2 requires prenylation (Figures 1A, 1C, and 2A, bottom panel), we sought to determine if the converse is true. We assessed prenylation by metabolic labeling with [^{3}H] mevalonate and found that palmitoylation-deficient FBXL2(C417S/C419S) was prenylated (Figures 2A, top panel, and S1B). This is consistent with the expectation that prenylation is required to bring FBXL2 into

proximity with a relevant membrane-associated palmitoyl acyltransferase for palmitoylation. In contrast, prenylation, which is catalyzed by cytosolic prenyltransferases, requires no prerequisite membrane affinity of substrates.

Both palmitoylation and prenylation are required for CaaX proteins (such as RAS) to dynamically localize to the PM and endomembranes. Time-lapse live-cell microscopy revealed that GFP-FBXL2 has access to the PM and motile vesicular compartments (Video S1). To determine the effects of prenylation and palmitoylation on FBXL2 membrane targeting, we investigated the subcellular distribution of FBXL2 by live-cell confocal imaging and subcellular fractionation. GFP-FBXL2 was observed at the PM and on cytoplasmic vesicles enriched in the perinuclear region (Figures 2B, top left panel, and 2C, top left panel; Video S1). Blocking prenylation with a geranylgeranyl transferase inhibitor (GGTi) rendered GFP-FBXL2 cytosolic, as demonstrated by the homogeneous fluorescence with negatively imaged organelles (Figure 2B, top middle panel). Like inhibition of prenylation, inhibition of palmitoylation with 2-bromopalmitate (2-BP) blocked delivery to the PM. However, rather than a cytosolic pattern, GFP-FBXL2 was observed on endomembranes in 2-BP-treated cells (Figure 2B, top right panel). Colocalization with ER Tracker but not Mito Tracker confirmed that this was the ER (Figures 2B, bottom panels, and S2A) but not mitochondria (Figure S2B). Palmitoylation-deficient GFP-FBXL2(C417S/C419S) was observed exclusively on the ER (Figures 2C, top right panel, and S2C; Video S2). GFP-FBXL2(C417S) localized similarly to GFP-FBXL2, whereas GFP-FBXL2(C419S) localized to endomembranes and, to a lesser extent, vesicles (Figure 2C, bottom panels; Videos S3 and S4). Subcellular fractionation using doxycycline-inducible Flp-In cells expressing FBXL2 at near endogenous levels confirmed that whereas FBXL2 is exclusively membrane associated (Figures 2D, lane 2, and S2D), prenylation-deficient GFP-FBXL2(C420S) is entirely cytosolic (Figure 2D, lane 7). Palmitoylation-deficient GFP-FBXL2(C417S/C419S) was recovered in both membrane and cytosolic compartments, consistent with diminished, but not absent, affinity for membranes (Figure 2D, lanes 4 and 8). That is, when palmitoylated, FBXL2 gains access to the PM, but when depalmitoylated, it resides on the ER. Since palmitoylation is readily reversible and the half-life of a palmitate modification is very short relative to that of the polypeptide, our results suggest that there is a pool of FBXL2 on both the PM and endomembrane and that the relative distribution is regulated by palmitoylation/depalmitoylation.

PDE6δ interacts with prenylated FBXL2 and together with palmitoylation regulates its delivery to specific membrane compartments

PDE6δ is a prenyl-protein binding protein that accommodates both farnesyl and geranylgeranyl lipid modifications in its hydrophobic binding pocket.[36,37] Mass spectrometric analysis of proteins immunoaffinity purified with FLAG-FBXL2 included PDE6δ (Table S1). We confirmed the interaction by co-immunoprecipitation of endogenous PDE6δ with FLAG-FBXL2 (Figure 3A, top panel). Because F box proteins such as FBXL2 possess WD repeats, leucine-rich regions, and other proteinprotein interaction domains that mediate binding to clients of the E3 ligase, we sought to determine if PDE6δ is among the clients of this family by including others in our co-immunoprecipitation assay. Of the 28 F box proteins, as well as the two APC/C substrate receptor subunits CDC20 and CDH1

tested, only FBXL2, the only one with a CaaX sequence, interacted with PDE6δ (Figures 3A and S3A). PDE6δ abundance and turnover was affected neither by the proteasome inhibitor MG132 (Figure S3B) nor silencing of FBXL2 (Figure S3C), confirming that PDE6δ is not a target of FBXL2-mediated proteasomal degradation but rather a regulator of FBXL2. The prenyl-binding capacity of PDE6δ can be disrupted by deleting exon 3 (Δexon 3), which encodes a portion of one of the hydrophobic β sheets and is a naturally occurring mutation in patients with Joubert syndrome.[38] Whereas FLAG-FBXL2, along with its core SCF partners Cul1 and SKP1, could be co-affinity purified with streptavidin-binding peptide (STREP)-tagged PDE6δ, these proteins did not bind STREP-PDE6δ(Δexon 3) (Figure 3B). Prenylation-deficient FLAG-FBXL2(C420S) did not interact with PDE6δ (Figure 3C, top panel, lane 2). Finally, deltarasin, a drug that binds in the hydrophobic pocket of PDE6δ and thereby inhibits the binding of prenyl-proteins,[39] blocked the interaction of FBXL2 with PDE6δ (Figures 3D and S3D). Interestingly, the apparent binding ability of PDE6δ for FBXL2 was greater than that for KRAS4B (Figure 3D), suggesting that either the geranylgeranyl modification drives higher binding ability and/or FBXL2 residues proximal to the prenylcysteine make contact with the prenyl-binding protein. Thus, FBXL2 is a binding partner of PDE6δ by virtue of the geranylgeranyl modification of FBXL2 and the prenyl-binding pocket of PDE6δ.

Whereas NRAS is a prenylated client of PDE6δ, HRAS is not.[40] Since both of these RAS proteins are dynamically palmitoylated, it remains uncertain how palmitoylation in proximity to the prenylcysteine held by PDE6δ affects the interaction. Palmitoylation-deficient FBXL2(C417S/C419S) bound more PDE6δ than wild-type FBXL2 (Figure 3C, top panel, lane 1 versus 3), suggesting that palmitoylation may inhibit the interaction of prenylated FBXL2 and PDE6δ or that the added affinity for membranes that palmitoylation affords FBXL2 prevents extraction, thereby inhibiting PDE6δ interaction.

PDE6δ mediates transfer through the aqueous environment of the cytosol of its client proteins from one membrane compartment to another.[37] This function can be assessed by extraction of client proteins such as NRAS, KRAS4B, and RHEB from membranes upon overexpression of PDE6δ.[21,40] We found that overexpression of mCherry-PDE6δ, but not mCherry-PDE6δ (Δexon 3), extracted GFP-FBXL2 from the PM and vesicles and rendered it cytosolic (Figures 3E andS3E). Whereas deltarasin inhibits the interaction between PDE6δ and prenyl-proteins, paradoxically, it blocks KRAS4B from associating with membranes because it interrupts the continuous cycling of KRAS4B between membrane compartments that is required for steady-state localization.[41] We found that inhibition of PDE6δ by either deltarasin or silencing its expression had the same effect on GFP-FBXL2 membrane association (Figures 3F, S3F, and S3G) as reported for KRAS4B, suggesting that the cycling of FBXL2 on and off membranes is also regulated by PDE6δ. Taken together, these results indicate that PDE6δ is a cytoplasmic chaperone required for the delivery and distribution of lipid-modified FBXL2 to membrane compartments.

Palmitoylation of FBXL2 and PDE6δ regulates substrate degradation at subcellular membrane compartments

We have shown that IP3R3, a calcium channel that resides exclusively in the ER, is one of the membrane-associated substrates for the E3 ligase activity of FBXL2.[27] Because we found that prenylated but depalmitoylated FBXL2 accumulates on the ER membrane (Figures 2, S2A, and S2C), whereas PDE6δ delocalizes FBXL2 from all membranes (Figure 3), we used the newly-generated depalmitoylated FBXL2 mutant and PDE6δ to investigate the impact of the subcellular distribution on substrate degradation at a specific subcellular compartment, the ER. As expected, core SCF components (Cul1 and SKP1) as well as IP3R3, a substrate, co-immunoprecipitated with FLAG-FBXL2 (Figure 4A, top panel, lane 1). In contrast, prenylation-deficient FLAG-FBXL2(C420S) captured Cul1 and SKP1 but not IP3R3, demonstrating that whereas prenylation is not required for the assembly of the core SCF E3 ligase complex, it is required for interaction with IP3R3. The inability of prenylation-deficient FLAG-FBXL2(C420S) to interact with IP3R3 is due to the loss of membrane association (including the ER) because of a lack of prenylation (Figure S4A). Importantly, prenylated but depalmitoylated FBXL2(C417S/C419S), which also interacted with Cul1 and SKP1, interacted more efficiently with IP3R3 than did wild-type FBXL2 (Figure 4A, top panel, lane 3). Consistent with this result, the steady-state IP3R3 levels were significantly reduced upon expression of the palmitoylation-deficient FBXL2(C417S/C419S) mutant but not the prenylation-deficient FBXL2(C420S) (Figure 4A, WCL top panel). Moreover, palmitoylation-deficient FBXL2(C417S/C419S) mutant promoted IP3R3 degradation more efficiently compared with wild-type FBXL2 (Figure S4B). Moreover, we investigated the impact of the subcellular distribution of FBXL2 on the neddylation of Cul1, a marker of substrate engagement for CRLs.[42] Neddylation of Cul1 in whole-cell lysates upon expression of FBXL2, FBXL2(C420S), FBXL2(C417S/C419S), PDE6δ, and PDE6δ(Δexon 3) was detected without any noticeable changes in the ratios of neddylated and non-neddylated forms (Figures 4A and 44B). Interestingly, we found that neddylated Cul1 was significantly diminished in the prenylation-deficient FBXL2(C420S) immune-complex relative to wild-type FBXL2 (Figures 4A, lanes 1 versus 2, and S4C), consistent with its inability to engage substrates including IP3R3 (Figure 4A, top panel, lane 2) outside of membrane compartments. In contrast, palmitoylation-deficient FBXL2(C417S/C419S) co-immunoprecipitated with neddylated Cul1, albeit to a lower extent compared with wild type (Figures 4A, lanes 1 versus 3, and S4C), suggesting that palmitoylation-deficient FBXL2 is still able to engage a subset of substrates at the ER. Furthermore, the proportion of neddylated Cullin-1 associated with FBXL2 was reduced upon FBXL2 delocalization from all membranes induced by PDE6δ overexpression (Figures 4B, 3E, and S3E).

Co-expression of FLAG-FBXL2 with STREP-PDE6δ, but not STREP-PDE6δ(Δexon 3), diminished the ability of FBXL2 to interact with IP3R3 (Figure 4B, top panel, lane 2), demonstrating that when FBXL2 is extracted from membranes by PDE6δ, it loses affinity for this substrate. Consequently, the degradation of IP3R3 was inhibited by PDE6δ overexpression but not PDE6δ(Δexon 3) (Figures 4B, WCL lane 2 versus 3, and S4D). Thus, the interaction of FBXL2 with IP3R3 is enhanced by membrane association and by depalmitoylation, a condition that targets FBXL2 to the ER, the membrane compartment where IP3R3 is resident.

At the ER, after binding, its physiological ligand IP3, IP3R3 (a calcium channel), is targeted by FBXL2 for degradation in response to oxidative stress and mitogen activation, regulating the ER-to-mitochondria calcium homeostasis.[27,28,43,44] To determine the functional effects of palmitoylation on the ability of FBXL2 to suppress IP3R3, we studied H_2O_2-stimulated calcium release from A549 cells or an A549 knockin cell line engineered to express the IP3R3(Q-FR/A-AA), a stable mutant that is not ubiquitylated by FBXL2.[27] Treatment with GGTi enhanced, and 2-BP inhibited, calcium release from parental A549 cells, whereas neither GGTi nor 2-BP had any effect on calcium release in cells expressing IP3R3(Q-FR/A-AA), demonstrating that altered localization of FBXL2 is correlated with altered IP3R3-dependent calcium release into cytosol (Figure 4C). We found that GGTi and 2-BP had similar effects on mitochondrial calcium flux in response to ATP (generating IP3 for IP3R3 activation) as measured by mitochondria-targeted aequorin (mtAEQ) (Figure S4E). Deltarasin had the same effect of GGTi, enhancing calcium release from parental A549 cells but not IP3R3(Q-FR/A-AA)-expressing cells (Figure S4G). These data demonstrate that whereas membrane association as a consequence of prenylation and PDE6δ-mediated shuttling is required for FBXL2 to regulate IP3R3 channel activity, palmitoylation negatively regulates the system. H_2O_2-stimulated calcium release from the ER through IP3R3 diminishes cell survival.[27,28,43,44] Substitution of FBXL2-insensitive IP3R3(Q-FR/A-AA) for the wild-type channel diminished the ability of A549 cells to survive the oxidative stress created by treatment with H_2O_2, and neither 2-BP nor GGTi had an effect on the survival of the IP3R3(Q-FR/A-AA)-expressing cells (Figure 4D). A549 cells expressing wild-type IP3R3 were more resistant to H_2O_2, and the resistance was diminished by GGTi but enhanced by 2-BP (Figure 4D). Consistent with these findings, PARP cleavage was reduced in 2-BP-treated cells but was increased in GGTi-treated cells, suggesting that FBXL2 palmitoylation/depalmitoylation and prenylation regulate apoptotic cell death (Figure S4F). Thus, membrane association on the ER as a consequence of depalmitoylation is required for the functional outcome of E3 ligase activity of FBXL2 toward IP3R3.

Depalmitoylation of FBXL2 in response to oxidative stress, in contrast to perturbing FBXL2 cycling by PDE6δ, improves cell survival by limiting IP3R3-mediated calcium efflux from the ER

If the substrate specificity of FBXL2 is regulated by palmitoylation/depalmitoylation-dependent targeting to membrane compartments, then conditions that call for enhanced FBXL2 activity at the ER should be associated with diminished palmitoylation. One such condition is oxidative stress, whereby FBXL2 enhances cell survival by depleting IP3R3 and thereby limiting the flux of calcium from the ER.[27] Indeed, we found that induction of oxidative stress with H_2O_2 resulted in diminished palmitoylation of FBXL2 without affecting FBXL2 protein levels (Figure 5A). We next determined the effects of lipidation mutants on the ability of FBXL2 to modulate H_2O_2-induced calcium flux in A549 cells expressing wild-type IP3R3 or FBXL2-resistant IP3R3(Q-FR/A-AA). Whereas prenylation-deficient FBXL2(C420S) enhances calcium flux, as it is unable to degrade IP3R3, palmitoylation-deficient FBXL2(C417S/C419S) reduces calcium flux due to increased IP3R3 degradation activity relative to wild-type FBXL2 in parental A549 cells (Figure 5B). Neither FBXL2 nor the two lipidation mutants affected calcium release in IP3R3(Q-FR/A-AA)-expressing cells (Figure 5B). When observing cell survival in response

to H_2O_2 treatment, we found that parental A549 cells expressing palmitoylation-deficient FBXL2(C417S/C419S) were more resistant to oxidative stress than prenylation-deficient and wild-type FBXL2 (Figure 5C). Thus, consistent with the effects of 2-BP (Figure 4C), palmitoylation of FBXL2 negatively regulates its activity toward IP3R3. Overexpression of PDE6δ, but not PDE6δ(Δexon 3), also interfered with the ability of FBXL2 to limit calcium release (Figure 5D) and support cell survival (Figure 5E) in cells expressing wild-type IP3R3 but not IP3R(Q-FR/A-AA). Similar effects of both the FBXL2 lipidation mutants and overexpression of PDE6δ were observed on mitochondrial calcium flux upon stimulation with ATP (Figure S5). These data demonstrate that palmitoylation of FBXL2 is negatively regulated by oxidative stress and that depalmitoylated FBXL2 mitigates that stress by engaging and degrading IP3R3 on the ER, thereby limiting calcium flux from that compartment and into mitochondria, a process inhibited by retention of FBXL2 in the cytosol by PDE6δ.

DISCUSSION

The regulation of spatially-restricted ubiquitylation is not well understood. For example, FBXL2-CRL engages substrates at several membrane compartments, but how its subcellular membrane targeting is regulated is unknown. We investigated the delivery and maintenance of spatial organization of FBXL2 as a prototypical model to gain insights into an example of compartmental substrate targeting via the UPS. Because CaaX proteins are known to be driven to the PM in conjunction with a second signal that most often consists of adjacent cysteines that are reversibly palmitoylated, we explored the possibility that membrane targeting of FBXL2 is regulated by cycles of palmitoylation/depalmitoylation. Our data demonstrate that this is the case. We further demonstrated that prenylated FBXL2 can be partitioned away from membranes by PDE6δ. We show that the interplay between FBXL2 palmitoylation and geranylgeranylation, as well as PDE6δ binding, is important for maintaining the dynamic compartmental organization of FBXL2-CRL to target substrates in response to specific cues.

FBXL2 is palmitoylated on two C-terminal cysteines (C417 and C419) (Figure 1D). Interestingly, the FBXL2(C419S) mutant, compared with FBXL2(C417S), displays a greater loss of palmitoylation (Figure 1D). Thus, although both cysteines contribute to FBXL2 palmitoylation, C419, located directly adjacent to the C420 prenylation site, is the predominant palmitoylation site in FBXL2. We found that FBXL2(C417S/C419S) was completely deficient in palmitoylation (Figure 1D, lane 2), showing that C417 and C419 are the sole palmitoylation sites for FBXL2. The analysis of the steady-state subcellular distribution of FBXL2 suggests that palmitoylation at C419, the predominant palmitoylation site, is required for FBXL2 localization to PM (Figure 2C; Video S4). Both palmitoylation-deficient FBXL2(C417S/C419S) and FBXL2(C419S) mutants are absent at the PM, whereas FBXL2(C417S) retains localization indistinguishable from wild type presumably because palmitoylation at C419 is intact (Figure 2C; Videos S1, S2, S3, and S4). Therefore, our results suggest that C419 may be a critical palmitoylation site that provides the second signal after prenylation for FBXL2 to traffic from Golgi/ER endomembranes to the PM, a paradigm similar to trafficking of palmitoylated RAS proteins (HRAS, NRAS, and KRAS4A).[10,13,14]

Our results also demonstrate that the lipid binding chaperone PDE6δ interacts with lipid-modified FBXL2 to facilitate its delivery to subcellular compartments. We propose that PDE6δ is responsible for trafficking FBXL2 to subcellular membrane compartments in a manner akin to RAS and related small GTPases such as RHEB.[21,45] RAS proteins are differentially engaged by PDE6δ, and the poor binding of HRAS to the chaperone is thought to be a function of steric hindrance by the proximal acyl chain in the case of HRAS.[40] Our observation that palmitoylation-deficient FBXL2(C417/419S) binds PDE6δ better than wild type (Figure 3C) suggests that palmitoylation of FBXL2 diminishes binding in a manner similar to HRAS. As has been extensively documented for small GTPases, lack of palmitoylation prevents the trafficking of FBXL2 from the ER to the PM, likely by vesicular transport. Lack of PDE6δ binding to FBXL2 also prevents FBXL2 trafficking to the PM (Figures 3F and S3F) but by a different mechanism. Loss of membrane association of a PDE6δ client upon discharge of the lipidated cargo from the cytosolic chaperone is somewhat counterintuitive. However, Bastiaens and colleagues have explained this phenomenon as due to disruption of unidirectional vesicular transport from a specific compartment coupled with a solubilization factor that combine to create a trafficking pathway that corrects for the entropic equilibration of RAS to all membranes.[46] Thus, like RAS, FBXL2 traffics between subcellular compartments including the PM and the ER in a manner regulated by both palmitoylation/depalmitoylation and PDE6δ binding.

PDE6δ is implicated in ciliopathies (e.g., Joubert syndrome) and RAS-mediated oncogenesis. Because of its clinical relevance, PDE6δ is a current target for drug design, and one promising tool compound, deltarasin, has been reported.[39] We found that FBXL2 binds PDE6δ with higher apparent affinity than does KRAS4B, suggesting that this class of drug will affect FBXL2 and its substrates. Indeed, we found that deltarasin had a profound effect on FBXL2 trafficking to the PM. Thus, in developing anti-PDE6δ agents, the biology of FBXL2 must be taken into consideration with regard to unwanted consequences and therapeutic index.

Facilitated by PDE6δ and the interplay of lipid modifications, FBXL2-CRL is able to maintain a dynamic spatial organization at the PM, vesicles, and the ER to regulate compartmental substrate targeting. Cullin-1 neddylation is widely believed to be a marker of substrate engagement by CRLs.[42] Neddylation was retained, albeit to a lesser extent, in the palmitoylation-deficient FBXL2(C417S/C419S) compared with wild type, consistent with its redistribution to the ER membrane compartment, where it may engage only a subset of substrates such as IP3R3 (Figures 4A and S4C). In contrast, neddylation of Cullin-1 associated with prenylation-deficient FBXL2(C420S) was negligible. Moreover, the proportion of neddylated Cullin-1 associated with FBXL2 was reduced when PDE6δ overexpression induced FBXL2 delocalization from membranes (Figures 4B, 3E, and S3E), suggesting that dissociation from all membrane compartments precludes substrate engagement consistent with the notion that substrate binding inhibits NEDD8 deconjugation of Cul1 by COP9 signalosome.[42]

The functional importance of regulating the lipid modifications of FBXL2 and resultant compartment-specific substrate degradation is highlighted by the increased degradation of IP3R3 by palmitoylation-deficient FBXL2(C417S/C419S) owing to its redistribution

to the ER compartment to counteract calcium-dependent cell death in response to H_2O_2 (Figures 4, S4B, and 5). Disruption of the PDE6δ-FBXL2 equilibrium inhibits FBXL2 membrane association, prevents IP3R3 degradation, and promotes cell death in response to H_2O_2 (Figures 3, 4, and 5). If critical FBXL2 functions such as protecting from cell death mediated by calcium flux through IP3R3 are regulated by palmitoylation/depalmitoylation of FBXL2, then the stresses that increase calcium flux must have an effect on FBXL2 palmitoylation. Importantly, we have shown such an effect by demonstrating that H_2O_2 induces depalmitoylation of FBXL2 (Figure 5A). These studies suggest that disruption of membrane associations to redistribute FBXL2 away from one or all membrane compartments by inhibiting prenylation, palmitoylation, and PDE6δ binding can serve as strategies to regulate compartment-specific targeting of substrates by FBXL2-CRL for therapeutic gain.

Finally, we propose a model based on our latest findings (Figure S6). Three cysteines (C417, C419, C420) in the C terminus of FBXL2 are post-translationally modified by lipids (Figures S6A and 1). Whereas C420 is modified by geranylgeranylation, both C417 and C419 are modified by palmitoylation (Figures S6A and 1). Unlike geranylgeranylation, palmitoylation is reversible. Palmitoylation of FBXL2 serves as a second signal to deliver geranylgeranylated-FBXL2 from the ER to the PM via an equilibrium established by vesicular transport and PDE6δ shuttling, which works against entropy (Figure S6A). The palmitoylation/depalmitoylation cycle and PDE6δ modulate FBXL2 cellular distribution and regulate FBXL2-mediated substrate degradation at specific subcellular compartments. Whereas FBXL2 palmitoylation enhances PM localization, FBXL2 depalmitoylation redistributes the ligase to the ER, allowing it to target ER-localized substrates such as IP3R3 calcium channels. In response to oxidative stress, IP3R3 channels open, resulting in persistent calcium flux from the ER to mitochondria that, if unopposed, leads to apoptosis due to mitochondrial calcium overload. To counter calcium-mediated cell death, oxidative stress promotes FBXL2 depalmitoylation and redistribution of FBXL2. Depalmitoylated FBXL2 accumulates at the ER to promote efficient IP3R3 ubiquitylation and subsequent p97-mediated proteasomal degradation of IP3R3, preventing persistent calcium flux from the ER and enhancing resilience to oxidative stress (Figure S6B)

Limitations of the study

This study identified C417 and C419 as palmitoylation sites in FBXL2; however, the current study lacks experimental evidence that FBXL2 is or is not simultaneously palmitoylated on both C417 and C419. However, the caveat to consider is that this study did not investigate if endogenous FBXL2 is palmitoylated. This study showed an apparent differential binding ability of PDE6δ for FBXL2 and KRAS4B but does not provide experimentally verified mechanism for this observation. That oxidative stress regulates FBXL2 palmitoylation is interesting observation; however, more rigorous analysis across various cell types with orthogonal approaches other than ABE was not performed in this study. Moreover, the mechanism of how oxidative stress regulates FBXL2 palmitoylation is unclear in this study. Further investigation is warranted to see if the rates of FBXL2 palmitoylation/depalmitoylation are regulated by oxidative stress. How palmitoylation regulates PDE6δ binding to FBXL2 is also unclear. Solving the crystal structure of the FBXL2-PDE6δ

complex will provide a better understanding of differential binding and the regulatory role of palmitoylation.

STAR★METHODS

RESOURCE AVAILABILITY

Lead contact—Any further inquiries or requests for the resources and reagents mentioned can be directed to the lead contact, Shafi Kuchay (kuchay@uic.edu).

Material availability—Plasmids and reagents generated in this study will be made available on request, but we may require a payment and/or a completed materials transfer agreement if there is potential for commercial application.

Data and code availability

- Data have been deposited at Mendeley and are publicly available as of the date of publication. DOIs are listed in the key resources table. Mass spectrometry data are publicly available *via* Kuchay et al., Nature, 2017. Link is listed in the key resources table.
- This paper does not report original code.
- Any additional information required to reanalyze the data reported in this paper is available from the lead contact upon request.

EXPERIMENTAL MODEL AND SUBJECT DETAILS

Cell lines—All cells, unless indicated, were grown in DMEM (Sigma) supplemented with 10% FBS (Corning) at 37°C with 5% CO_2 and regularly tested for mycoplasma. Flp-In T-REx 293 cells were sourced from ThermoFisher. All other cells were sourced from the American Type Culture Collection. HEK 293T cells were female, A549 cells were male, HeLa cells were female, and COS-7 cells were male.

METHOD DETAILS

Generation of FBXL2 Flp-In cell lines—FLAG-tagged FBXL2 wild-type, FBXL2(C420S) and FBXL2(C417S/C419S) inserts were obtained by restriction digestion from their respective pcDNA3 constructs and subcloned into pcDNA™5/FRT/TO (Invitrogen) by using HindIII and NotI (Invitrogen) restriction sites compatible between the two vectors. Individual constructs were co-transfected with pOG44 (Flp recombinase expression plasmid, Invitrogen) into the Flp-In™ T-Rex™-293 cell line (Invitrogen) containing a single integrated FRT (FLP Recombination Target) site and stably expressing the Tet repressor. FRT site present in the vector is required for its Flp recombinase mediated integration into the Flp-In™ T-Rex™ host cell line. Hygromycin (160 μg/mL) was used for the selection of positive cells. Doxycycline (2 μg/mL) was added to the medium for inducing gene expression.

Subcellular fractionation—Subcellular fractionation of cells to yield PM, cytosolic, and ER was performed according to.[47] Briefly, treated or transfected HEK-293T cells were

trypsinized and resuspended in buffer (225 mM mannitol, 75mM sucrose, 0.1 mM EDTA, 30 mM Tris pH 7.4) and processed by Dounce homogenization. Large cell debris was cleared by centrifugation 3 times at 600 × g for 5 min. Crude mitochondrial fraction was pelleted at 10,000 x g for 10 min. The supernatant was centrifuged at 100,000 × g for 1 h to separate the membrane fraction (pellet) from the cytosolic fraction. Fractions were lysed using lysis buffer and processed for immunoblotting.

Palmitoylation assay

Metabolic labeling with [^{3}H] palmitate: Labeling and detection of palmitoylation was performed according to.[48] Briefly, HEK 293T cells were seeded into a 6 well dish in DMEM with 10% dialyzed FBS supplemented with 5 mM sodium pyruvate and 3.6 mg/mL BSA. GFP and FLAG-tagged constructs of FBXL2 and HRAS were transfected into cells using Lipofectamine 2000 with the manufacturer's recommended instructions. 0.2 mCi/mL of [^{3}H] palmitic acid was used to label cells for 16 h. Cells were collected and lysed in RIPA buffer (20 mM Tris, pH 7.5, 137 mM NaCl, 2 mM EDTA, 0.5% sodium deoxycholate, 0.1% SDS, 1% NP-40, 10% glycerol, c0mplete protease inhibitor cocktail (Roche)). Denatured cell lysates were immunoprecipitated with anti-GFP and anti-FLAG agarose resin respectively. Immunoprecipitations were analyzed by SDS-PAGE, autoradiography, and immunoblotting. For autoradiography, the membrane was placed under a phosphor screen (28-9564-82, Cytiva) for two weeks and the screen was exposed in a phosphor imager (Amersham Typhoon, GE) for [^{3}H] detection. The PVDF membrane was finally blotted for construct expression using rabbit anti-FLAG antibody (F7425-Sigma).

Acyl-biotin exchange: Detection of palmitoylation was carried out as described.[49] Briefly, HEK-293T cells were transfected with GFP-tagged FBXL2 using PEI for 14 h. After lysis in lysis buffer supplemented with 0.1% SDS, denatured whole cell extracts were immunoprecipitated using anti-GFP resin. Samples were blocked in lysis buffer (pH 7.4) supplemented with 50 mM N-ethylmaleimide for 12 h. Half of the beads were then treated with 1M hydroxylamine in lysis buffer (pH 7.4) for 1 h, while the other half were left untreated as control. Beads were incubated in lysis buffer (pH 6.5) containing 2 μM biotin-BMCC (Invitrogen). Samples were boiled in 2X sample buffer at 95°C for 5 min and immunoblotted with Strepavidin-HRP (Pierce).

Prenylation assay—HEK 293T cells were grown in 6 cm dishes and treated with 15 μM lovastatin (M2147-25MG, Sigma) for about 2 h. Fresh medium containing 400 μCi of mevalonolactone RS-[5-3H] (ART 0315A, ARC) and 15 μM lovastatin was added. Cells were then transiently transfected with FLAG-tagged FBXL2(C417S/C419S) and FBXL2(C420S). After overnight incubation, cells were harvested and lysed with Nonidet P-40 substitute (Roche)-based lysis buffer containing protease inhibitor cocktail (Roche) and sonicated (Sonic Dismembrator, Fisher Scientific). A portion of the lysate was taken as input and the rest was clarified using Protein G Agarose (Invitrogen) followed by overnight immunoprecipitation with anti-flag M2 affinity gel (A2220-Sigma). After washing the M2 gel, elution was carried out with 2X Bolt LDS sample buffer (novex). The samples were run on Bolt 4–12% Bis-Tris Plus gel (Invitrogen) and transferred onto PVDF membrane (Millipore). The membrane was placed under a phosphor screen (28-9564-82, Cytiva) for

two weeks and the screen was exposed in a phosphor imager (Amersham Typhoon, GE) for [^{3}H] detection. The PVDF membrane was finally immunoblotted for FLAG-tagged FBXL2(C417S/C419S) and FBXL2 (C420S) expression using rabbit anti-FLAG antibody (F7425-Sigma).

Live-cell imaging—HeLa cells (~1×10^5) were plated on glass bottom dishes (ThermoFisher) and transiently transfected using Lipofectamine 3000 (Invitrogen) for 14 h. For movies, cells were recorded for 1 h, taking one frame every 3 min (total 20 frames). Imaging was performed using a Zeiss LSM-700 confocal microscope at 63X using the oil-immersion objective. Images were processed using ImageJ.

Fura-2 measurements—The cytosolic Ca^{2+} response was evaluated using the fluorescent Ca^{2+} indicator Fura-2/AM (Thermo Fischer Scientific). In brief, cells were grown on 24-mm coverslips and incubated at 37C for 30 min in 1 mM Ca^{2+} in Krebs–Ringer buffer (KRB: 135 mM NaCl, 5 mM KCl, 1 mM $MgSO_4$, 0.4 mM K_2HPO_4, 5.5 mM glucose, 20 mM HEPES) supplemented with 2.5 mM Fura-2/AM, 0.02% Pluronic F-68 (Sigma-Aldrich), and 0.1 mM sulfinpyrazone (Sigma- Aldrich). Parental A549 cells or A549 knock-in clones were transfected with FBXL2 or PDE6δ constructs or treated with GGTi-2418 (50 mM for 24 h), 2-BP (50 mM for 24 h) or deltarasin (5 or 10 mM for 3 h). Cells were then washed and supplied with 1 mM Ca^{2+}/KRB. To determine cytosolic Ca^{2+} response, the cells were placed in an open Leyden chamber on a 37°C thermostated stage and exposed to 340/380 nm wavelength light using the Olympus xCellence (Olympus) multiple wavelength high-resolution fluorescence microscopy system equipped with a Hamamatsu ORCA ER CCD camera (Hamamatsu Photonics) and an Upl FLN 40× oil objective (Olympus) to determine the cytosolic Ca^{2+} response. H_2O_2 (1 mM) was added to the 1 mM Ca^{2+}/Krebs-Ringer buffer. The fluorescence data collected were expressed as emission ratios at 340/380 nm. In the figures, the kinetics of the cytosolic Ca^{2+} responses after H_2O_2 stimulation are presented as the ratio of fluorescence at 340/380 nm in cells loaded with Fura-2/AM.

Aequorin measurements—COS-7 cells grown on 13-mm round glass coverslips were transfected with the aequorin (mitochondria-targeted aequorin, mtAEQ) together with the indicated plasmid. Cells were starved for 20h in 0.1% FBS and serum-stimulated with DMEM supplemented with 10% FBS for 4 h. Where indicated, cells were treated with GGTi-2418 (50mM for 24 h) or 2-BP (75 mM for 24 h). Cells were reconstituted with coelenterazine for 1.5 h in Krebs–Ringer modified buffer (KRB; 125 mM NaCl, 5 mM KCl, 1 mM Na_3PO_4, 1 mM $MgSO_4$, 5.5 mM glucose, and 20 mM 4-(2-hydroxyethyl)-1-piperazineethanesulfonic acid [HEPES], pH 7.4, at 37°C) supplemented with 1 mM $CaCl_2$, and then transferred to the perfusion chamber. All aequorin measurements were carried out in KRB supplemented with 1 mM $CaCl_2$ and the agonist was added to the same medium as indicated in figure legends. The experiments were terminated by lysing the cells with Triton X-100 in a hypotonic Ca^{2+}-rich solution (10 mM $CaCl_2$ in H_2O), thus discharging the remaining aequorin pool. The light signal was collected and calibrated into [Ca^{2+} values by an algorithm based on the Ca^{2+} response curve of aequorin at physiological conditions of pH, [Mg^{2+}], and ionic strength, as previously described.[50]

Cellular viability—The cellular viability was evaluated using the calcein assay, which is based on the conversion of the cell permeant non-fluorescent calcein AM dye to the fluorescent calcein dye by intracellular esterase activity in live cells. Briefly, A549 cells or A549 knock-in clones were plated into black sided clear bottom 96-well microplates and transfected with FBXL2 or PDE6δ constructs or treated with GGTi-2418 (50 mM for 24 h), 2-BP (75 mM for 24 h) as indicated. Cells were then washed and treated with 1mM H2O2 for 6 h in DMEM supplemented with 10% FBS. Cells were then incubated with 1 mM calcein AM at 37°C for 30 min, after which fluorescence at 485 nm was determined using GloMax Discover Detection System (Promega Corporation U.S.A.).

Gene silencing—HEK-293T cells were transfected with 5 nM ON-TARGETplus siRNA (Dharmacon) using Lipofectamine RNAiMAX (Invitrogen) according to the manufacturer's instructions for 48–72 h. The following siRNA oligos from Dharmacon were used: ON-TARGETplus human FBXL2 (J-013562-05-005), ON-TARGETplus human PDE6δ (J-004310-10-005), ON-TARGETplus Non-targeting Control Pool (D-001810-10-05).

Immunoprecipitation, immunoblotting and transfections—Transfections were performed using polyethylenimine (Polysciences), Lipofectamine 3000 (Invitrogen), or Lipofectamine RNAiMAX (Invitrogen) according to the manufacturer's instructions. Cells were treated with deltarasin (Cayman Chemicals), 2-bromopalmitate ((2BP) Sigma), and GGTi-2418 and cycloheximide (Sigma) as indicated. HEK-293T cells were transiently transfected using polyethylenimine (Polysciences) for 14 h. Pellets were lysed in lysis buffer (50 mM Tris pH 8.0, 150 mM NaCl, 0.1% NP-40, 50 mM NaF, 1 mM EDTA, 10% glycerol). Lysate was pre-cleared using Protein G Agarose (Invitrogen) for 1 h at 4°C rocking. Total lysates were then immunoprecipitated with either anti-FLAG M2 (Sigma) or anti-GFP (MBL) conjugated resin for 90 min at 4°C rocking. Samples were eluted in 2X Laemmli sample buffer (Sigma) and boiled at 95°C for 5 min before SDS-PAGE and immunoblotting. Cleaved PARP levels were analyzed in A549 cells or A549 knock-in clones treated with either vehicle or H_2O_2 500 mM overnight in DMEM supplemented with 10% FBS. When indicated, A549 cells were transfected with FBXL2 or PDE6δ constructs for 36 h or treated with GGTi-2418 (50 mM for 24 h), 2-BP (50 mM for 24 h) as indicated in the figure legends.

QUANTIFICATION AND STATISTICAL ANALYSIS

Western blot quantification was done using ImageJ. Pearson's correlation coefficient for colocalization was calculated using the Zeiss blue analysis software. Statistical analysis was performed used GraphPad Prism 9. Unless otherwise stated in the figure legends, experiments were performed in biological triplicates (n = 3). When comparing multiple groups, two-way ANOVA was performed to determine significance, and the Tukey test for multiple comparisons was used post hoc to determine significance between groups. Unpaired Student's t-test was performed when comparing only two groups. Significance was defined as * = $p < 0.05$, ** = $p < 0.01$, *** = $p < 0.001$, *** = $p < 0.0001$ unless otherwise stated in the figure legends. Error bars shown represent the standard error of the mean (SEM).

Supplementary Material

Refer to Web version on PubMed Central for supplementary material.

ACKNOWLEDGMENTS

The authors acknowledge Michele Pagano and Paolo Pinton for inputs on results and manuscript preparations. This work was supported by grants from the National Institutes of Health (R35 GM137452 to S.K. and R35 CA253178, R01 CA211687, and RO1 CA163489 to M. Philips) and Fondazione Telethon ETS, Italy (to D.G.), as well as funds provided by the BCMG department at UIC to S.K.

INCLUSION AND DIVERSITY

We support inclusive, diverse, and equitable conduct of research.

REFERENCES

1. Harper JW, and Schulman BA (2021). Cullin-RING ubiquitin ligase regulatory circuits: a quarter century beyond the F-box hypothesis. Annu. Rev. Biochem. 90, 403–429. 10.1146/annurev-biochem-090120-013613. [PubMed: 33823649]
2. Petroski MD, and Deshaies RJ (2005). Function and regulation of cullin-RING ubiquitin ligases. Nat. Rev. Mol. Cell Biol. 6, 9–20. [PubMed: 15688063]
3. Pohl C, and Dikic I (2019). Cellular quality control by the ubiquitin-proteasome system and autophagy. Science 366, 818–822. 10.1126/science.aax3769. [PubMed: 31727826]
4. Skaar JR, Pagan JK, and Pagano M (2013). Mechanisms and function of substrate recruitment by F-box proteins. Nat. Rev. Mol. Cell Biol. 14, 369–381. 10.1038/nrm3582. [PubMed: 23657496]
5. Skaar JR, Pagan JK, and Pagano M (2009). Snap-Shot: F box proteins I. Cell 137, 1160–1160.e1. [PubMed: 19524517]
6. Skaar JR, D'Angiolella V, Pagan JK, and Pagano M (2009). Snap-Shot: F box proteins II. Cell 137, 1358 e1351. [PubMed: 19563764]
7. Casey PJ (1995). Protein lipidation in cell signaling. Science 268, 221–225. 10.1126/science.7716512. [PubMed: 7716512]
8. Jiang H, Zhang X, Chen X, Aramsangtienchai P, Tong Z, and Lin H (2018). Protein lipidation: occurrence, mechanisms, biological functions, and enabling technologies. Chem. Rev. 118, 919–988. 10.1021/acs.chemrev.6b00750. [PubMed: 29292991]
9. Wang M, and Casey PJ (2016). Protein prenylation: unique fats make their mark on biology. Nat. Rev. Mol. Cell Biol. 17, 110–122. 10.1038/nrm.2015.11. [PubMed: 26790532]
10. Campbell SL, and Philips MR (2021). Post-translational modification of RAS proteins. Curr. Opin. Struct. Biol. 71, 180–192. 10.1016/j.sbi.2021.06.015. [PubMed: 34365229]
11. Linder ME, and Deschenes RJ (2007). Palmitoylation: policing protein stability and traffic. Nat. Rev. Mol. Cell Biol. 8, 74–84. 10.1038/nrm2084. [PubMed: 17183362]
12. Roberts PJ, Mitin N, Keller PJ, Chenette EJ, Madigan JP, Currin RO, Cox AD, Wilson O, Kirschmeier P, and Der CJ (2008). Rho Family GTPase modification and dependence on CAAX motif-signaled posttranslational modification. J. Biol. Chem. 283, 25150–25163. 10.1074/jbc.M800882200. [PubMed: 18614539]
13. Choy E, Chiu VK, Silletti J, Feoktistov M, Morimoto T, Michaelson D, Ivanov IE, and Philips MR (1999). Endomembrane trafficking of ras: the CAAX motif targets proteins to the ER and Golgi. Cell 98, 69–80. 10.1016/S0092-8674(00)80607-8. [PubMed: 10412982]
14. Michaelson D, Silletti J, Murphy G, D'Eustachio P, Rush M, and Philips MR (2001). Differential localization of Rho GTPases in live cells: regulation by hypervariable regions and RhoGDI binding. J. Cell Biol. 152, 111–126. 10.1083/jcb.152.1.111. [PubMed: 11149925]
15. Goodwin JS, Drake KR, Rogers C, Wright L, Lippincott-Schwartz J, Philips MR, and Kenworthy AK (2005). Depalmitoylated Ras traffics to and from the Golgi complex via a nonvesicular pathway. J. Cell Biol. 170, 261–272. 10.1083/jcb.200502063. [PubMed: 16027222]

16. Cook TA, Ghomashchi F, Gelb MH, Florio SK, and Beavo JA (2000). Binding of the delta subunit to rod phosphodiesterase catalytic subunits requires methylated, prenylated C-termini of the catalytic subunits. Biochemistry 39, 13516–13523. 10.1021/bi001070l. [PubMed: 11063588]

17. Gillespie PG, Prusti RK, Apel ED, and Beavo JA (1989). A soluble form of bovine rod photoreceptor phosphodiesterase has a novel 15-kDa subunit. J. Biol. Chem. 264, 12187–12193. [PubMed: 2545702]

18. Cherfils J, and Zeghouf M (2013). Regulation of small GTPases by GEFs, GAPs, and GDIs. Physiol. Rev. 93, 269–309. 10.1152/physrev.00003.2012. [PubMed: 23303910]

19. Hoffman GR, Nassar N, and Cerione RA (2000). Structure of the Rho family GTP-binding protein Cdc42 in complex with the multifunctional regulator RhoGDI. Cell 100, 345–356. 10.1016/s0092-8674(00)80670-4. [PubMed: 10676816]

20. Zhang H, Constantine R, Frederick JM, and Baehr W (2012). The prenyl-binding protein PrBP/delta: a chaperone participating in intracellular trafficking. Vision Res. 75, 19–25. 10.1016/j.visres.2012.08.013. [PubMed: 22960045]

21. Ismail SA, Chen YX, Rusinova A, Chandra A, Bierbaum M, Gremer L, Triola G, Waldmann H, Bastiaens PIH, and Wittinghofer A (2011). Arl2-GTP and Arl3-GTP regulate a GDI-like transport system for farnesylated cargo. Nat. Chem. Biol. 7, 942–949. 10.1038/nchem-bio.686. [PubMed: 22002721]

22. Zhang H, Constantine R, Vorobiev S, Chen Y, Seetharaman J, Huang YJ, Xiao R, Montelione GT, Gerstner CD, Davis MW, et al. (2011). UNC119 is required for G protein trafficking in sensory neurons. Nat. Neurosci. 14, 874–880. 10.1038/nn.2835. [PubMed: 21642972]

23. Kuchay S, Duan S, Schenkein E, Peschiaroli A, Saraf A, Florens L, Washburn MP, and Pagano M (2013). FBXL2- and PTPL1-mediated degradation of p110-free p85beta regulatory subunit controls the PI(3)K signalling cascade. Nat. Cell Biol. 15, 472–480. 10.1038/ncb2731. [PubMed: 23604317]

24. Koga K, Yao I, Setou M, and Zhuo M (2017). SCRAPPER selectively contributes to spontaneous release and presynaptic long-term potentiation in the anterior cingulate cortex. J. Neurosci. 37, 3887–3895. 10.1523/JNEUROSCI.0023-16.2017. [PubMed: 28292828]

25. Yao I, Takagi H, Ageta H, Kahyo T, Sato S, Hatanaka K, Fukuda Y, Chiba T, Morone N, Yuasa S, et al. (2007). SCRAPPER-dependent ubiquitination of active zone protein RIM1 regulates synaptic vesicle release. Cell 130, 943–957. 10.1016/j.cell.2007.06.052. [PubMed: 17803915]

26. Han S, Lear TB, Jerome JA, Rajbhandari S, Snavely CA, Gulick DL, Gibson KF, Zou C, Chen BB, and Mallampalli RK (2015). Lipopolysaccharide primes the NALP3 inflammasome by inhibiting its ubiquitination and degradation mediated by the SCFFBXL2 E3 ligase. J. Biol. Chem. 290, 18124–18133. 10.1074/jbc.M115.645549. [PubMed: 26037928]

27. Kuchay S, Giorgi C, Simoneschi D, Pagan J, Missiroli S, Saraf A, Florens L, Washburn MP, Collazo-Lorduy A, Castillo-Martin M, et al. (2017). PTEN counteracts FBXL2 to promote IP3R3- and Ca(2+)-mediated apoptosis limiting tumour growth. Nature 546, 554–558. 10.1038/nature22965. [PubMed: 28614300]

28. Kuchay S, Saeed M, Giorgi C, Li J, Hoffmann HH, Pinton P, Rice CM, and Pagano M (2018). NS5A promotes constitutive degradation of IP3R3 to counteract apoptosis induced by hepatitis C virus. Cell Rep. 25, 833–840.e3. 10.1016/j.celrep.2018.09.088. [PubMed: 30355490]

29. Lai CY, Ho YC, Hsieh MC, Wang HH, Cheng JK, Chau YP, and Peng HY (2016). Spinal fbxo3-dependent Fbxl2 ubiquitination of active zone protein RIM1alpha mediates neuropathic allodynia through CaV2.2 activation. J. Neurosci. 36, 9722–9738. 10.1523/JNEURO-SCI.1732-16.2016. [PubMed: 27629721]

30. Lin TB, Hsieh MC, Lai CY, Cheng JK, Chau YP, Ruan T, Chen GD, and Peng HY (2015). Fbxo3-Dependent Fbxl2 ubiquitination mediates neuropathic allodynia through the TRAF2/TNIK/GluR1 cascade. J. Neurosci. 35, 16545–16560. 10.1523/JNEUROSCI.2301-15.2015. [PubMed: 26674878]

31. Niu M, Xu J, Liu Y, Li Y, He T, Ding L, He Y, Yi Y, Li F, Guo R, et al. (2021). FBXL2 counteracts Grp94 to destabilize EGFR and inhibit EGFR-driven NSCLC growth. Nat. Commun. 12, 5919. 10.1038/s41467-021-26222-x. [PubMed: 34635651]

32. Kuchay S, Wang H, Marzio A, Jain K, Homer H, Fehrenbacher N, Philips MR, Zheng N, and Pagano M (2019). GGTase3 is a newly identified geranylgeranyltransferase targeting a ubiquitin ligase. Nat. Struct. Mol. Biol. 26, 628–636. 10.1038/s41594-019-0249-3. [PubMed: 31209342]
33. Wang C, Gale M Jr., Keller BC, Huang H, Brown MS, Goldstein JL, and Ye J (2005). Identification of FBL2 as a geranylgeranylated cellular protein required for hepatitis C virus RNA replication. Mol. Cell 18, 425–434. [PubMed: 15893726]
34. Chen BB, Coon TA, Glasser JR, and Mallampalli RK (2011). Calmodulin antagonizes a calcium-activated SCF ubiquitin E3 ligase subunit, FBXL2, to regulate surfactant homeostasis. Mol. Cell Biol. 31, 1905–1920. 10.1128/MCB.00723-10. [PubMed: 21343341]
35. Chen BB, Coon TA, Glasser JR, McVerry BJ, Zhao J, Zhao Y, Zou C, Ellis B, Sciurba FC, Zhang Y, and Mallampalli RK (2013). A combinatorial F box protein directed pathway controls TRAF adaptor stability to regulate inflammation. Nat. Immunol. 14, 470–479. 10.1038/ni.2565. [PubMed: 23542741]
36. Dharmaiah S, Bindu L, Tran TH, Gillette WK, Frank PH, Ghirlando R, Nissley DV, Esposito D, McCormick F, Stephen AG, and Simanshu DK (2016). Structural basis of recognition of farnesylated and methylated KRAS4b by PDEdelta. Proc. Natl. Acad. Sci. USA 113, E6766–E6775. 10.1073/pnas.1615316113. [PubMed: 27791178]
37. Baehr W (2014). Membrane protein transport in photoreceptors: the function of PDEdelta: the Proctor lecture. Invest. Ophthalmol. Vis. Sci. 55, 8653–8666. 10.1167/iovs.14-16066. [PubMed: 25550383]
38. Thomas S, Wright KJ, Le Corre S, Micalizzi A, Romani M, Abhyankar A, Saada J, Perrault I, Amiel J, Litzler J, et al. (2014). A homozygous PDE6Δ mutation in Joubert syndrome impairs targeting of farnesylated INPP5E protein to the primary cilium. Hum. Mutat. 35, 137–146. 10.1002/humu.22470. [PubMed: 24166846]
39. Zimmermann G, Papke B, Ismail S, Vartak N, Chandra A, Hoffmann M, Hahn SA, Triola G, Wittinghofer A, Bastiaens PIH, and Waldmann H (2013). Small molecule inhibition of the KRAS-PDEdelta interaction impairs oncogenic KRAS signalling. Nature 497, 638–642. 10.1038/nature12205. [PubMed: 23698361]
40. Tsai FD, Lopes MS, Zhou M, Court H, Ponce O, Fiordalisi JJ, Gierut JJ, Cox AD, Haigis KM, and Philips MR (2015). K-Ras4A splice variant is widely expressed in cancer and uses a hybrid membrane-targeting motif. Proc. Natl. Acad. Sci. USA 112, 779–784. 10.1073/pnas.1412811112. [PubMed: 25561545]
41. Schmick M, Vartak N, Papke B, Kovacevic M, Truxius DC, Rossmannek L, and Bastiaens PIH (2014). KRas localizes to the plasma membrane by spatial cycles of solubilization, trapping and vesicular transport. Cell 157, 459–471. 10.1016/j.cell.2014.02.051. [PubMed: 24725411]
42. Liu X, Reitsma JM, Mamrosh JL, Zhang Y, Straube R, and Deshaies RJ (2018). Cand1-Mediated adaptive exchange mechanism enables variation in F-box protein expression. Mol. Cell 69, 773–786.e6. 10.1016/j.molcel.2018.01.038. [PubMed: 29499133]
43. Oberdorf J, Webster JM, Zhu CC, Luo SG, and Wojcikiewicz RJ (1999). Down-regulation of types I, II and III inositol 1,4,5-trisphosphate receptors is mediated by the ubiquitin/proteasome pathway. Biochem. J. 339, 453–461. [PubMed: 10191279]
44. Orrenius S, Zhivotovsky B, and Nicotera P (2003). Regulation of cell death: the calcium-apoptosis link. Nat. Rev. Mol. Cell Biol. 4, 552–565. 10.1038/nrm1150. [PubMed: 12838338]
45. Philips MR (2012). Ras hitchhikes on PDE6δelta. Nat. Cell Biol. 14, 128–129. 10.1038/ncb2429. [PubMed: 22298042]
46. Schmick M, Kraemer A, and Bastiaens PIH (2015). Ras moves to stay in place. Trends Cell Biol. 25, 190–197. 10.1016/j.tcb.2015.02.004. [PubMed: 25759176]
47. Wieckowski MR, Giorgi C, Lebiedzinska M, Duszynski J, and Pinton P (2009). Isolation of mitochondria-associated membranes and mitochondria from animal tissues and cells. Nat. Protoc. 4, 1582–1590. 10.1038/nprot.2009.151. [PubMed: 19816421]
48. Tsai FD, Wynne JP, Ahearn IM, and Philips MR (2014). Metabolic labeling of Ras with tritiated palmitate to monitor palmitoylation and depalmitoylation. Methods Mol. Biol. 1120, 33–41. 10.1007/978-1-62703-791-4_3.

49. Brigidi GS, and Bamji SX (2013). Detection of protein palmitoylation in cultured hippocampal neurons by immunoprecipitation and acyl-biotin exchange (ABE). J. Vis. Exp., 50031. 10.3791/50031. [PubMed: 23438969]

50. Bonora M, Giorgi C, Bononi A, Marchi S, Patergnani S, Rimessi A, Rizzuto R, and Pinton P (2013). Subcellular calcium measurements in mammalian cells using jellyfish photoprotein aequorin-based probes. Nat. Protoc. 8, 2105–2118. 10.1038/nprot.2013.127. [PubMed: 24113784]

Highlights

- FBXL2 is palmitoylated in a prenylation-dependent manner on C417 and C419 near the CaaX motif
- Palmitoylated FBXL2 decorates plasma membrane, whereas depalmitoylated FBXL2 is enriched at ER
- PDE6δ, a RAS-oncoprotein transporter, traffics lapidated FBXL2 to subcellular compartments
- FBXL2 subcellular distribution impacts spatially-restricted substrate degradation and apoptosis

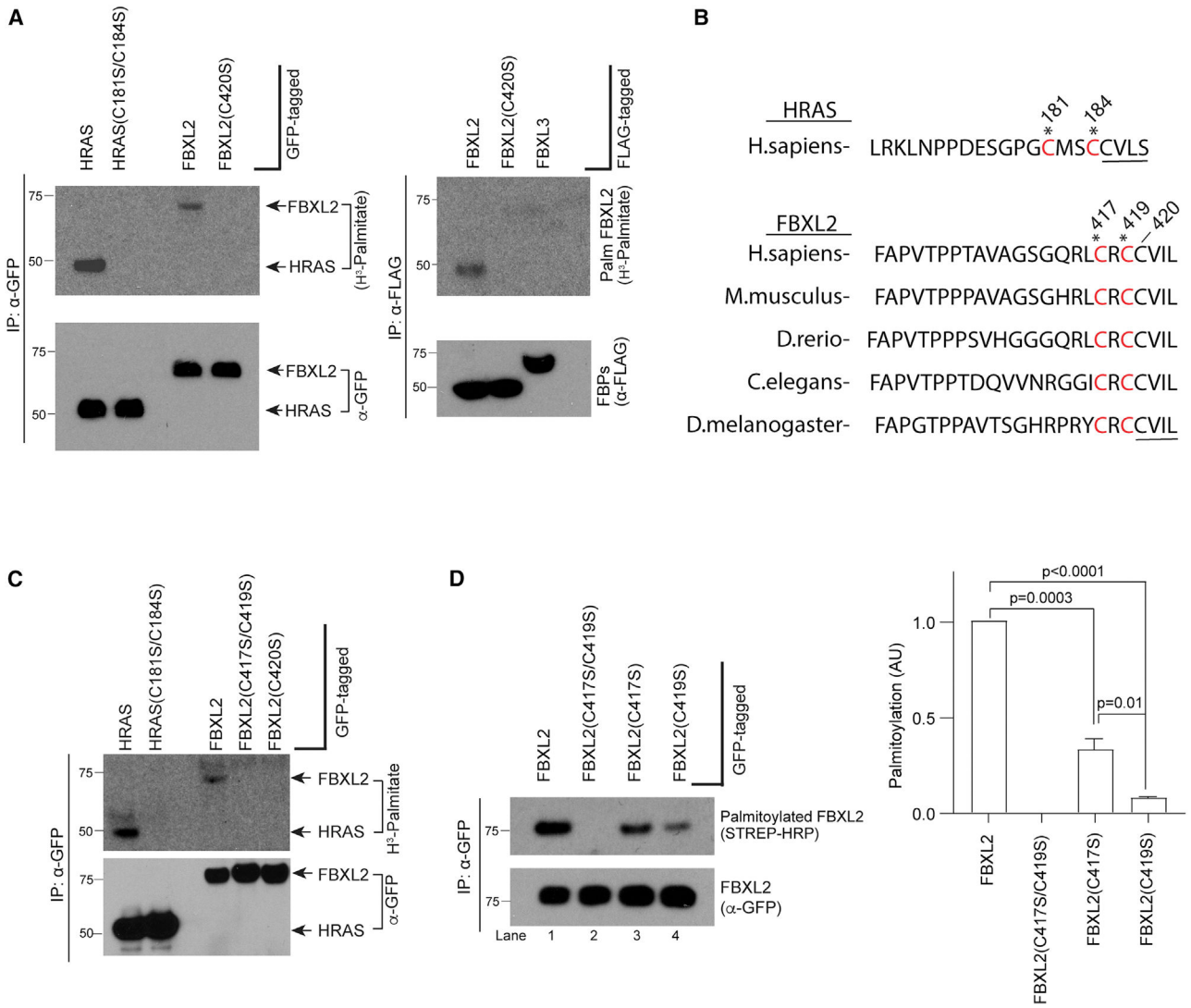

Figure 1. The F box protein FBXL2 is palmitoylated at cysteines 417 and 419

(A) FBXL2, but not FBXL2(C420S), is palmitoylated. Indicated tagged versions of FBXL2, FBXL2(C420S), HRAS, HRAS(C181S/C184S), and FBXL3 were transfected in HEK-293T cells and metabolically labeled with [^{3}H]-palmitic acid. Clarified and denatured cell lysates were subjected to anti-GFP and anti-FLAG immunoprecipitations. As indicated, immunoprecipitates were resolved by SDS-PAGE and subjected to either autoradiography (top panels) or immunoblotting (bottom panels) as shown.

(B) FBXL2 palmitoylation sites are conserved across species. The alignment of C-terminal amino acid sequences of FBXL2 orthologs is shown. Predicted palmitoylation sites are indicated by asterisks (*). The CaaX motif is underlined. The numerals on top represent position from the N terminus. The C-terminal sequence for HRAS, a known palmitoylated protein, is shown on top for comparison.

(C) FBXL2, but not FBXL2(C417S/C419S) and FBXL2(C420S), is palmitoylated. GFP-tagged FBXL2, FBXL2(C417S/C419S), FBXL2(C420S), HRAS, and HRAS(C181S/

C184S) were transfected in HEK-293T cells, metabolically labeled with [^{3}H]-palmitic acid, and processed as in (A).

(D) FBXL2 is differentially palmitoylated at cysteines 417 and 419. GFP-tagged FBXL2, FBXL2(C417S/C419S), FBXL2(C417S), and FBXL2(C419S) were expressed in HEK-293T cells and immunoprecipitated using anti-GFP agarose resin. Washed immunoprecipitates were subject to acyl-biotin exchange palmitoylation assay (see STAR Methods for details). The reactions were analyzed by SDS-PAGE and immunoblotting as indicated. Bar graph shows the quantification of palmitoylation, represented as fold change compared with wild-type FBXL2 (lane 1) which was set to 1, in three independent experiments. p values were calculated by a one-way ANOVA and multiple-comparisons test. Error bars indicate SEM. AU, arbitrary units.

See also Figure S1.

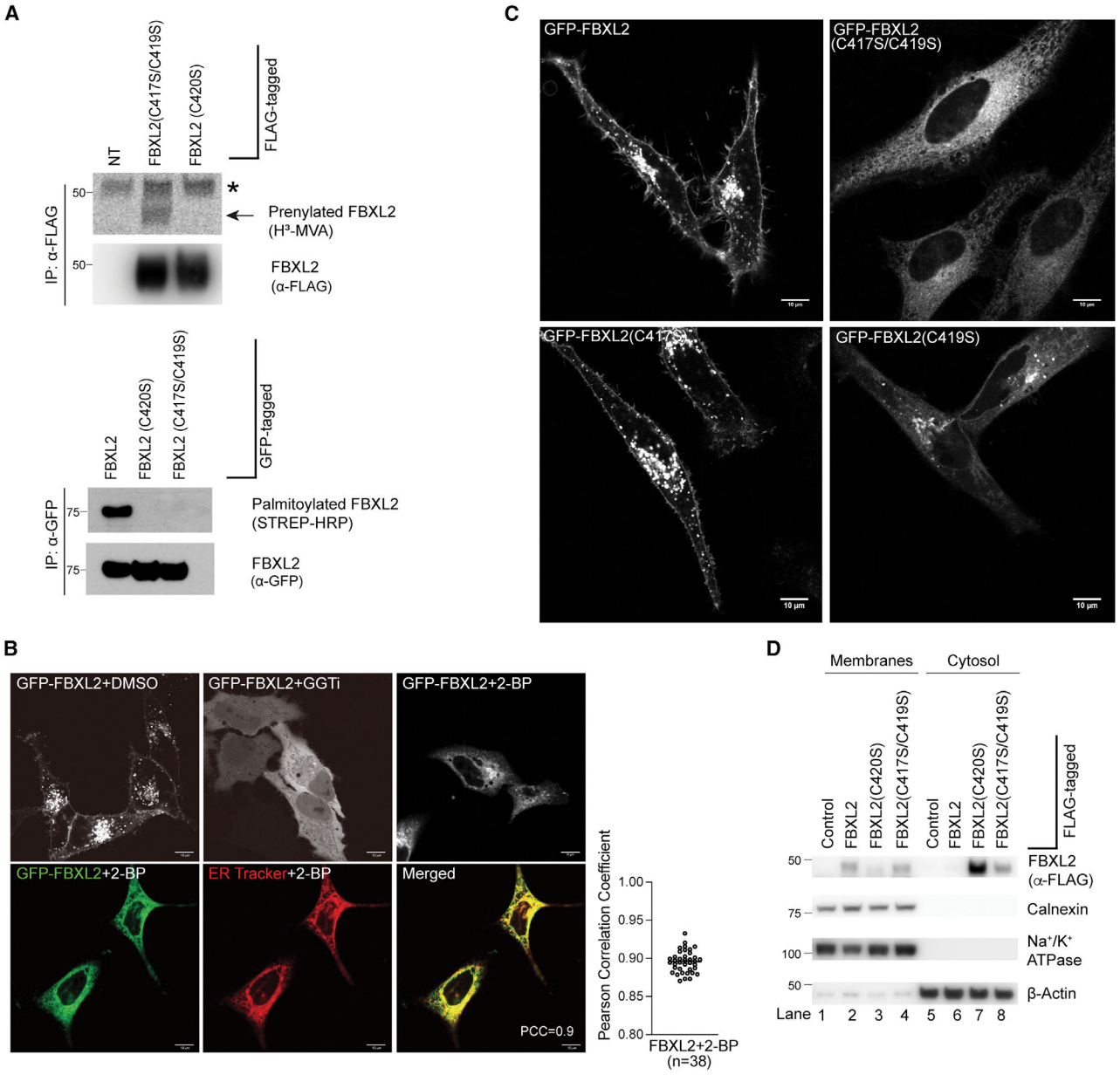

Figure 2. Palmitoylation is prenylation dependent, and its loss redistributes FBXL2 to ER

(A) FBXL2 prenylation is necessary for its palmitoylation, but not vice versa. Top: cells were treated with lovastatin for 2 h prior to FLAG-FBXL2(C420S) and FLAG-FBXL2(C417S/C419S) expression and simultaneous overnight labeling with mevalonolactone RS-[5-^{3}H]. Harvested cells were lysed and immunoprecipitated using anti-FLAG resin. Immunoprecipitates were analyzed by SDS-PAGE and subject to either autoradiography (top) or immunoblotting (bottom). Bottom: acyl-biotin exchange palmitoylation assay for GFP-tagged FBXL2, FBXL2(C420S), and FBXL2(C417S/C419S) was carried out as in Figure 1D. Asterisk indicates non specific band.

(B) Inhibition of palmitoylation, but not geranylgeranylation, redistributes FBXL2 to ER membranes. HeLa cells expressing GFP-FBXL2 were incubated with DMSO (top left),

geranylgeranylation inhibitor GGTi-2418 (top middle), and palmitoylation inhibitor 2-BP (top right and bottom panels) for 14 h. Live-cell confocal images captured by LSM700 confocal microscope are shown. Bottom panel: in 2-BP treated cells, ER Tracker was added 15 min before imaging to decorate the ER. Pearson correlation coefficient for colocalization with ER Tracker upon 2-BP treatment was analyzed in different cells (n = 38). Scale bar, 10 μM.

(C) Palmitoylation-deficient FBXL2 (C417S/C419S) decorates ER membranes. Live-cell confocal microscopy of HeLa cells expressing GFP-tagged FBXL2, FBXL2(C417S/C419S), FBXL2(C417S), and FBXL2(C419S) were carried out by ZEISS LSM700 confocal microscope. Representative images of three independent experiments are shown. Scale bar, 10 μM.

(D) Palmitoylation-deficient FBXL2 (C417S/C419S), but not prenylation-deficient FBXL2(C420S), is retained in membrane fractions. Flp-In 293 cells were established to allow doxycycline-induced expression of FLAG-tagged FBXL2, FBXL2(C420S), and FBXL2(C417S/C419S) at near physiological levels. Postinduction cells were harvested and subjected to subcellular fractionation using stepwise ultracentrifugation (see STAR Methods). Membrane and cytosolic fractions were subjected to SDS-PAGE and immunoblotted as indicated.

See also Figure S2.

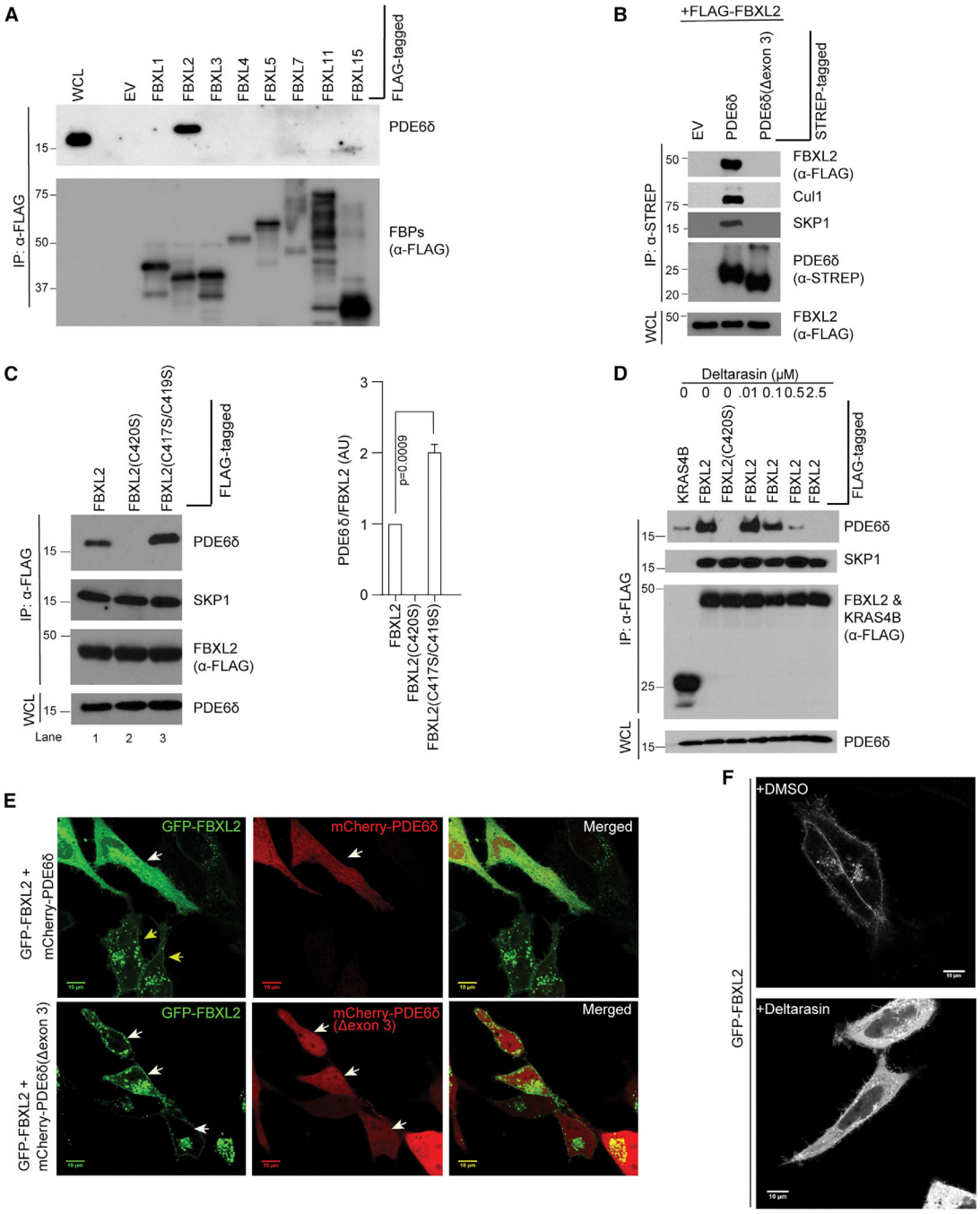

Figure 3. The lipid-binding chaperone PDE6δ interacts with FBXL2 and regulates its delivery to membrane compartments

(A) PDE6δ binds specifically to FBXL2. FLAG-tagged constructs of indicated F box proteins were expressed, and anti-FLAG immunoprecipitations were carried out with standard protocols. F box protein immunocomplexes were subject to SDS-PAGE and immunoblotting as shown. Shown is representative of three independent experiments. (B) Joubert syndrome-associated PDE6δ(Δexon 3) mutant does not bind to FBXL2. STREP-tagged PDE6δ and Joubert syndrome-associated mutant PDE6δ(Δexon 3) were

co-expressed with FLAG-FBXL2 and immunoprecipitated using anti-STREP resin. The immunocomplexes were subjected to SDS-PAGE and immunoblotted as indicated.

(C) FBXL2 palmitoylation regulates its binding to PDE6δ. FLAG-tagged FBXL2, FBXL2(C420S), and FBXL2(C417S/C419S) were expressed, and anti-FLAG immunoprecipitations were carried out. The immunocomplexes and whole-cell lysates were subjected to SDS-PAGE and immunoblotted as indicated. Shown is representative of three independent experiments. Bar graph shows quantification of PDE6δ binding to FBXL2 and its indicated mutants represented as a fold change compared with FBXL2 wild type (lane 1), which was set to 1. p values were calculated by one-way ANOVA and multiple-comparisons test. Error bars indicate SEM. AU, arbitrary units.

(D) FBXL2 binds PDE6δ more efficiently than KRAS4B, an interaction inhibited by deltarasin. FLAG-tagged FBXL2, FBXL2(C420S), and KRAS4B were expressed, and cells were treated with either DMSO or increasing doses of deltarasin as indicated. Immunoprecipitations were performed with anti-FLAG agarose resin, and immunocomplexes were subjected to SDS-PAGE followed by immunoblotting, as indicated. Shown is representative of three independent experiments.

(E) Disturbing the equilibrium between FBXL2 and PDE6δ, but not PDE6δ(Δexon 3), extracts FBXL2 from membranes. Live-cell confocal microscopy of mCherry-tagged PDE6δ and PDE6δ(Δexon 3) co-expressed with GFP-FBXL2 was captured by Zeiss LSM700 confocal microscope. Top panels: white arrows indicate delocalization of GFP-FBXL2 in cells co-expressing mCherry-PDE6δ. Yellow arrows indicate typical FBXL2 distribution in cells without mCherry-PDE6δ co-expressed. Bottom panel: mCherry-PDE6δ(Δexon 3) fails to delocalize FBXL2 in cells co-expressing GFP-FBXL2. Shown is representative of three independent experiments. Scale bar, 10 μM.

(F) Deltarasin treatment delocalizes FBXL2 from membrane compartments. Live-cell confocal microscopy of HeLa cells expressing GFP-FBXL2 treated with either DMSO or deltarasin was performed using Zeiss LSM700 confocal microscope. Shown is representative of three independent experiments. Scale bar, 10 μM.

See also Figure S3 and Table S1.

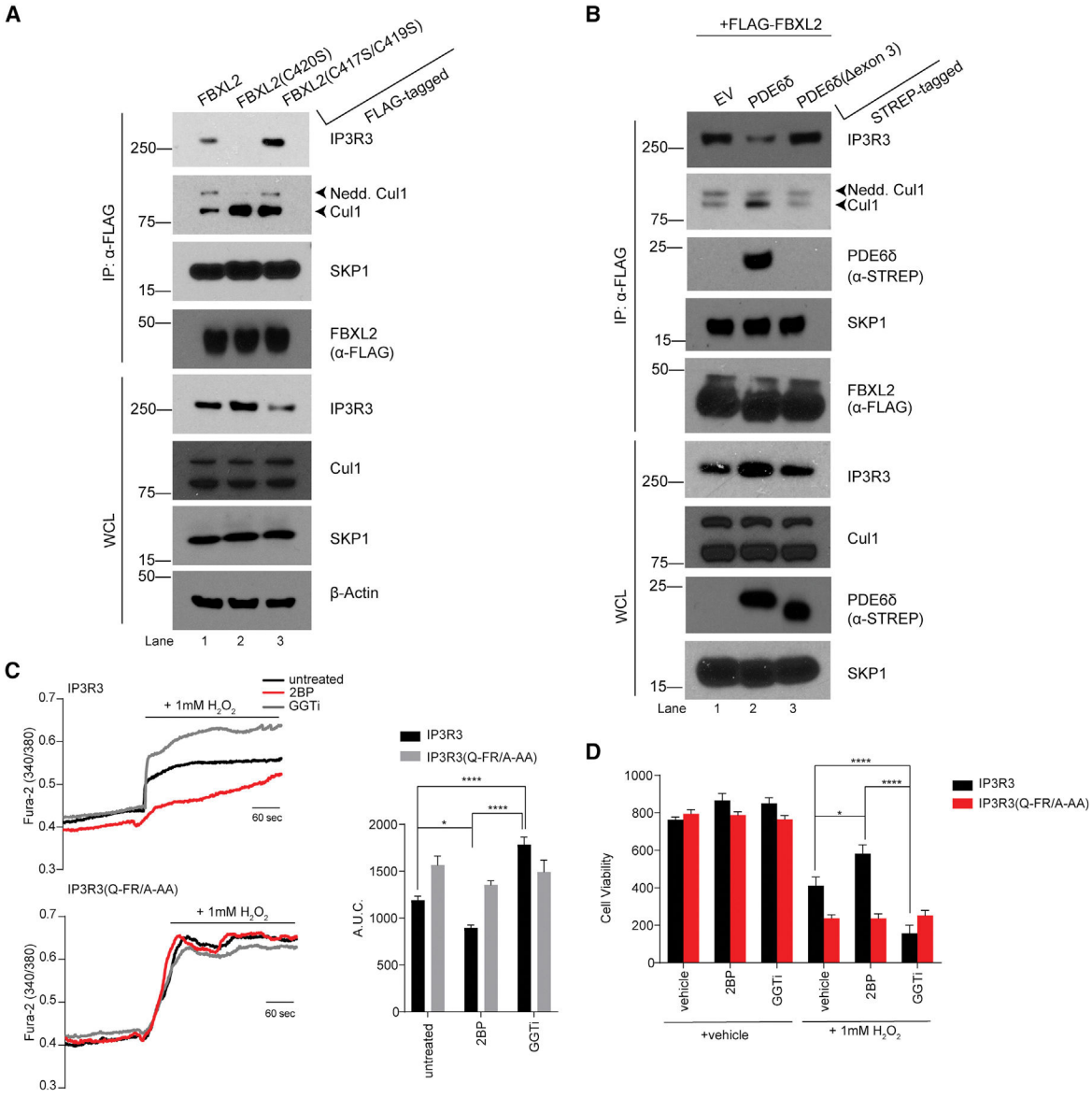

Figure 4. Palmitoylation and PDE6δ regulate FBXL2 substrate engagement and degradation at specific subcellular compartments

(A) FBXL2 deficient in palmitoylation, but not geranylgeranylation, promotes binding and degradation of ER-resident calcium channel IP3R3. FLAG-taggedFBXL2, FBXL2(C420S), and FBXL2(C417S/C419S) were expressed and immunoprecipitated with anti-FLAG agarose resin. The immunocomplexes and whole-cell lysates were subjected to SDS-PAGE and immunoblotting as indicated. Shown is representative of three independent experiments. (B) PDE6δ, but not Joubert syndrome-associated PDE6δ(Δexon 3), inhibits IP3R3 binding and degradation. STREP-tagged PDE6δ and PDE6δ(Δexon 3) were co-expressed with FLAG-FBXL2 as indicated, and immunoprecipitations were performed with anti-FLAG agarose resin. The immunocomplexes and whole-cell lysates were subjected to SDS-PAGE and immunoblotted as indicated. Shown is representative of three independent experiments.

(C) Pharmacological inhibition of palmitoylation decreases IP3R3-mediated calcium mobilization. Parental A549 cells and knockin cells expressing an FBXL2-insensitive IP3R3(Q-FR/A-AA) were treated with palmitoylation inhibitor 2-BP and geranylgeranyltransferase inhibitor GGTi-2418. Cytosolic Ca^{2+} levels were measured with the Ca^{2+}-sensitive fluorescent dye Fura-2 in response to H_2O_2 stimulation. The kinetic behavior of the $[Ca^{2+}]_c$ (Ca^{2+} concentration within the cytoplasm) response is presented as the ratio of fluorescence at 340/380 nm. Left panels show representative traces, and the panels on their right show quantifications of three independent experiments representing the area under the curve (AUC) measurements. p values were calculated by a one-way ANOVA and multiple-comparisons test. Error bars indicate SEM.

(D) Pharmacological inhibition of palmitoylation promotes cell survival via IP3R3 degradation. Parental A549 and knockin cells expressing FBXL2-insensitiveIP3R3(Q-FR/A-AA) were treated with 2-BP and GGTi-2418. Indicated amounts of H_2O_2 were added to cells, and post-6 h of treatment cell viability was evaluated using calcein assay, determining fluorescence at 485 nm. p values were calculated by a one-way ANOVA and multiple-comparisons test. Error bars indicate SEM. Shown is representative of three independent experiments.

See also Figure S4.

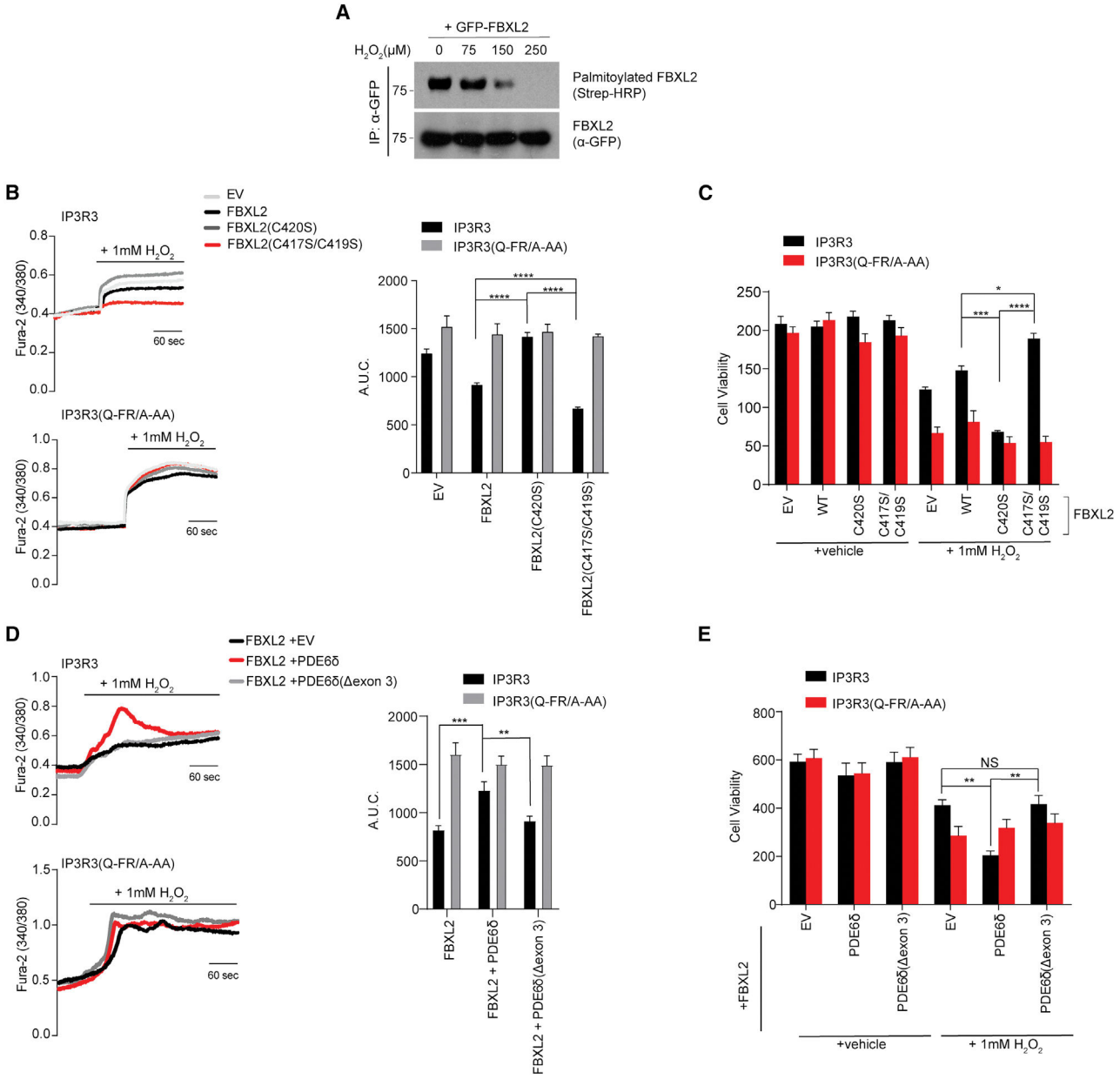

Figure 5. FBXL2 palmitoylation and PDE6δ regulate calcium-mediated cell death response to oxidative stress

(A) Oxidative stress decreases FBXL2 palmitoylation. GFP-FBXL2 was expressed in HEK-293T cells, and cells were treated with indicated doses of H_2O_2 for 4 h before cell harvesting and lysis. Denatured cell lysates were used for immunoprecipitations with anti-GFP agarose resin. Acyl-biotin exchange palmitoylation assay was performed on immunoprecipitates as in Figure 1D. The processed immunoprecipitations were analyzed with SDS-PAGE and immunoblotting as shown. Shown is representative of three independent experiments.

(B) Palmitoylation-deficient FBXL2(C417S/C419S) efficiently counteracts IP3R3-mediated calcium mobilization. FLAG-tagged FBXL2, FBXL2(C420S), and FBXL2(C417S/C419S) were expressed in parental A549 cells or knockin cells with FBXL2-insensitive IP3R3(Q-

FR/A-AA). Cytosolic Ca^{2+} levels were measured with Fura-2 AM using standard ratiometric analysis in response to indicated H_2O_2 stimulation as in Figure 4C. Representative individual calcium traces are shown (left side panels). Bar graph shows quantifications of three independent experiments representing the AUC measurements. p values were calculated by a one-way ANOVA and multiple-comparisons test. Error bars indicate SEM.

(C) Palmitoylation-deficient FBXL2(C417S/C419S) promotes cell survival via IP3R3 in response to oxidative stress. FLAG-tagged FBXL2, FBXL2(C420S), and FBXL2(C417S/C419S) were expressed in parental A549 cells or knockin cells with FBXL2-insensitive IP3R3(Q-FR/A-AA). H_2O_2 was added to cells as indicated, and 6 h post-treatment cell viability was determined using calcein assay as in Figure 4D. p values were calculated by a one-way ANOVA and multiple-comparisons test. Error bars indicate SEM. Shown is representative of three independent experiments.

(D) PDE6δ expression, but not PDE6δ(Δexon3), regulates IP3R3-mediated calcium flux. STREP-PDE6δ or STREP-PDE6δ(Δexon 3) were co-expressed with FBXL2 in parental A549 cells or knockin cells with FBXL2-insensitive IP3R3(Q-FR/A-AA). Cytosolic Ca^{2+} levels were processed and analyzed as in Figure 4C. p values were calculated by a one-way ANOVA and multiple-comparisons test. Error bars indicate SEM.

(E) PDE6δ expression, but not PDE6δ(Δexon3), regulates IP3R3-mediated cell survival in response to oxidative stress. STREP-PDE6δ or STREP-PDE6δ(Δexon3) were co-expressed with FBXL2 in parental A549 cells or knockin cells with FBXL2-insensitive IP3R3(Q-FR/A-AA). H_2O_2 was added to cells as indicated, and 6 h post-treatment cell viability was determined with calcein assay as in Figure 4D. p values were calculated by a one-way ANOVA and multiple-comparisons test.

Error bars indicate SEM. Shown is representative of three independent experiments.

See also Figures S5 and S6.

KEY RESOURCES TABLE

REAGENT or RESOURCE Antibodies	SOURCE	IDENTIFIER
Strep (1: 1,000 dilution)	IBA	Cat# 2-1507-001
PDE6δ (1:1,000 dilution)	MyBioSource	Cat# MBS7005086
IP3R3 (1:3,000 dilution)	Bethyl	Cat# A302-160A
GFP (1:1,000 dilution)	Cell Signaling Technology	Cat# 2959
FLAG (1:1,000 dilution)	Sigma-Aldrich	Cat# F3165
Anti-FLAG mAb (1:1,000 dilution)	Sigma-Aldrich	Cat# F1804
Streptavidin-HRP (1:5,000 dilution)	ThermoFisher Scientific	Cat# 21130
CUL1 (1:1,000 dilution)	Invitrogen	Cat# 71-8700
SKP1 (1:1,000 dilution)	Cell Signaling Technology	Cat# 12248
cleaved PARP (1:1,000 dilution)	Cell Signaling Technology	Cat# 9541
Na^+/K^+ ATPase (1:1,000 dilution)	Sigma-Aldrich	Cat# A276
β-Actin (1:10,000 dilution)	Sigma-Aldrich	Cat# A1978
Calnexin (1:1,000 dilution)	Santa Cruz Biotechnology	Cat# sc-23954
p27 (1:1,000 dilution)	BD-Transduction Laboratories	Cat# 610242
Rabbit-HRP	Invitrogen	Cat# NA934V
Mouse-HRP	Invitrogen	Cat# NA931V
Streptavidin-HRP	Pierce	Cat# 21126
Chemicals, peptides, and recombinant proteins		
GGTi-2418	Millipore	Cat# 345878
2-Bromopalmitate (2BP)	Sigma	Cat# 238422-10G
Deltarasin	Cayman Chemicals	Cat# 1440898-82-7
EZ-Link™BMCC-Biotin	ThermoFisher Scientific	Cat# 21900
Calcein AM	ThermoFisher Scientific	Cat# 65-0853-39
Hydrogen peroxide solution	Sigma-Aldrich	Cat# H1009
Adenosine 5'-triphosphate disodium salt hydrate (ATP)	Sigma-Aldrich	Cat# A7699
ER-Tracker™ Red	Invitrogen	Cat# E34250
MitoTracker™ Red	Invitrogen	Cat# M7512
Hygromycin	Sigma-Aldrich	Cat# H3274-1G
Doxycycline	Sigma-Aldrich	Cat# D9891
Upofectamine™ 2000 Transfection Reagent	ThermoFisher Scientific	Cat# 11668019
[^{3}H] palmitic acid	PerkinElmer	Cat# NET043001MC
Cycloheximide	Sigma-Aldrich	Cat# C7698
Anti-GFP (Green Fluorescent Protein) mAb-Agarose	MBL International Corporation	Cat# D153-8
PEI	polysciences	Cat# 23966
N-ethylmaleimide	Sigma-Aldrich	Cat# E3876-5G
Hydroxylamine	Sigma-Aldrich	Cat# 467804-10ML
Lovastatin	Sigma	Cat# M2147-25MG
Mevalonolactone RS-[5-3H]	ARC	Cat# ART0315A

REAGENT or RESOURCE Antibodies	SOURCE	IDENTIFIER
Nonidet P-40 substitute	Roche	Cat# 34619600
Protein G Agarose	Invitrogen	Cat# 15920010
anti-flag M2 affinity gel	Sigma	Cat# A2220
Lipofectamine 3000 Transfection Reagent	Invitrogen	Cat# L3000015
Fura-2/AM	Thermo Fischer Scientific	Cat# F1221
Pluronic F-68	Sigma-Aldrich	Cat# 9003-11-6
Sulfinpyrazone	Sigma- Aldrich	Cat# 57-96-5
Lipofectamine RNAiMAX Transfection Reagent	ThermoFisher Scientific	Cat# 13778150
Deposited data		
Raw data	This paper	https://doi.org/10.17632/jx8gty5cz8.1
Mass Spec data	Kuchay et al, Nature 2017[27]	ftp://odr.stowers.org/LIBPB-484. The link is accessible by downloading FTP client software such as FileZilla.
Experimental models: Cell lines		
HEK-293T	ATCC	Cat# CRL-3216
HeLa	ATCC	Cat# CCL-2
COS-7	ATCC	Cat# CRL-1651
A549 IP3R3(Q-FR/A-AA) knock-in clones	Kuchay et al, Nature 2017[27]	N/A
Flp-In™ T-REx™-293 cell line	Invitrogen	Cat# R78007
A549 cells	ATCC	Cat# CCL-185
Oligonucleotides		
ON-TARGETplus human FBXL2 (J-013562-05-005)	Dharmacon Kuchay et al, Nature 2017[27]	N/A
ON-TARGETplus human PDE6S (J-004310-10-005)	Dharmacon Kuchay et al, Nature 2017[27]	N/A
PDE6δ(Δexon 3) primer_Forward 5'-CTGGTGTGGAGCATGAGGAATGGTTCTTCGAGTTTG-3'	Integrated DNA Technology, USA	N/A
PDE6δ(Δexon 3) primer_ Reverse 5'- CAAACTCGAAGAACCATTCCTCATGCTCCACACCAG-3'	Integrated DNA Technology, USA	N/A
FBXL2(C417S) primer_Forward 5' - GACACAGCACCTGCTCAGTCGCTGTCCAC-3'	Integrated DNA Technology, USA	N/A
FBXL2(C417S) primer_Reverse 5' - GTGGACAGCGACTGAGCAGGTGCTGTGTC-3'	Integrated DNA Technology, USA	N/A
FBXL2(C419S) primer_Forward 5' - AGAGAATGACACAGCTCCTGCACAGTCGCTG-3'	Integrated DNA Technology, USA	N/A
FBXL2(C419S) primer_Reverse 5'- CAGCGACTGTGCAGGAGCTGTGTCATTCTCT-3'	Integrated DNA Technology, USA	N/A
FBXL2(C417S/C419S) primer_Forward 5'- GAGAATGACACAGCTCCTGCTCAGTCGCTGTCCAC-3'	Integrated DNA Technology, USA	N/A
FBXL2(C417S/C419S) primer_Reverse 5'- GTGGACAGCGACTGAGCAGGAGCTGTGTCATTCTC-3'	Integrated DNA Technology, USA	N/A
Recombinant DNA		

REAGENT or RESOURCE Antibodies	SOURCE	IDENTIFIER
FLAG-tagged FBXL2 wild-type	Kuchay et al, Nature Cell Biology, 2013[23]	N/A
FLAG-FBXL2(C420S)	Kuchay et al, Nature 2017[27]	N/A
FLAG-FBXL2(C417S/C419S)	This work	N/A
FLAG-FBXL2(C417S)	This work	N/A
FLAG-FBXL2(C419S)	This work	N/A
GFP-tagged FBXL2 wild-type	Kuchay et al, Nature Cell Biology, 2013[23]	N/A
GFP-FBXL2(C420S)	Kuchay et al, Nature Cell Biology, 2013[23]	N/A
GFP-FBXL2(C417S/C419S)	This work	N/A
GFP-FBXL2(C417S)	This work	N/A
GFP-FBXL2(C419S)	This work	N/A
pmCherry-PDE6δ	This work	N/A
pmCherry-PDE6δ ΔE3	This work	N/A
STREP-PDE6δ	This work	N/A
STREP -PDE6δ ΔE3	This work	N/A
pOG44 (Flp-recombinase expression plasmid)	Invitrogen	Cat# V600520
Software and algorithms		
ImageJ 1.49V	ImageJ	https://imagej.nih.gov
GraphPad 9.0	GraphPad Prism	http://www.graphpad.com
Adobe Illustrator 2019	Adobe	N/A
ZEISS ZEN 3.0 (blue edition)	Zeiss	N/A